Supplement of Atmos. Chem. Phys., 25, 9249–9262, 2025
https://doi.org/10.5194/acp-25-9249-2025-supplement

Atmospheric Chemistry and Physics
Open Access

Supplement of

Competing multiple oxidation pathways shape atmospheric limonene-derived organonitrates simulated with updated explicit chemical mechanisms

Qinghao Guo et al.

Correspondence to: Jialei Zhu (zhujialei@tju.edu.cn)

Section S1. Sensitivity simulations for limonene-derived ON using box model

A series of sensitivity tests were conducted using chemical box model. The initial concentration for the three oxidants is categorized into low (1.0×10^{5} molecules·cm^{-3} for OH, 1.0×10^{11} molecules·cm^{-3} for O_3, 1.0×10^{9} molecules·cm^{-3} for NO_3), medium (1.0×10^{11} molecules·cm^{-3} for OH, 1.0×10^{15} molecules·cm^{-3} for O_3, 1.0×10^{13} molecules·cm^{-3} for NO_3) and high (1.0×10^{19} molecules·cm^{-3} for OH, 1.0×10^{18} molecules·cm^{-3} for O_3, 1.0×10^{17} molecules·cm^{-3} for NO_3) levels for analysis in experiments with multiple initial oxidation pathways of limonene.

Sensitivity tests under multiple initial oxidation pathways could be divided into two sets. The first set of simulations was denoted as individual initial oxidation pathway cases, model was performed with only one initial oxidation pathway of limonene (OH-, O_3- or NO_3-initiated oxidation). In the experiments with OH-initiated oxidation pathway, low to high level of initial concentration of OH was added into chemical box model. In the experiments with O_3-initiated oxidation pathway, initial O_3 concentration ranging from low to high level was set. Similarly, in the experiments with NO_3-initiated oxidation pathway, low to high level initial concentration of NO_3 was set. The second set of simulations was denoted as multiple initial oxidation pathways cases, two and three initial oxidation pathways of limonene were included in chemical box model. These experiments intended to elucidate the synergistic effect of multiple initial oxidation pathways. In the experiments of OH + O_3 initiated oxidation pathway, low to high level initial concentrations of OH and O_3 were added into chemical box model. In the experiments of OH + NO_3 initiated oxidation pathway, additional initial OH and NO_3 concentrations ranging from low to high level were set for comparison of an initial concentration of 0 molecules cm^{-3}. Similarly, the experiments of O_3 + NO_3 initiated oxidation pathway with low to high level initial concentrations of O_3 and NO_3 were performed. Lastly, the experiments of OH + O_3 + NO_3 initiated oxidation pathway with low to high level initial concentrations of OH, O_3 and NO_3 were conducted. To ensure adequate intermediate reaction processes during the experiments, the initial concentration of other gaseous species included in chemical mechanism used in experiments were set to high enough. Experiments including OH-initiated oxidation pathway added an additional concentration of NO_3, NO and HO_2, experiments including O_3-initiated oxidation pathway added an additional concentration of OH, NO_3, NO, CO, SO_2, HO_2 and H_2O and experiments including NO_3-initiated oxidation pathway need to add initial concentrations of OH, NO and HO_2. Multiple initial oxidation pathway experiments included

OH-initiated, O_3-initiated or NO_3-initiated oxidation pathways, where the concentration of this oxidant was set according to the three initial concentration gradients mentioned above. The initial concentration of these gaseous species (OH, NO_3, NO, CO, SO_2, HO_2, H_2O) were set to 1.0×10^{10}, 1.0×10^{12}, 1.0×10^{12}, 1.0×10^{14}, 1.0×10^{10}, 1.0×10^{11} and 1.0×10^{16} molecules·cm^{-3}, respectively.

Section S2. **Sensitivity simulations for global atmospheric ON using global model**

We conducted sensitivity simulations to evaluate the impacts of oxidation pathways on burden of limonene-derived ON. The base case (Case0) includes all three initial oxidation pathways (OH-, O_3- and NO_3-initiated oxidation) to form limonene-derived ON. The first sensitivity case (Case1) was designed to examine the effects of OH-initiated oxidation pathway on global limonene-derived ON formation. In Case1, the model was run in the same way as Case0 but without OH-initiated oxidation pathway of limonene. The second sensitivity case (Case2) was designed to examine the effects of O_3-initiated oxidation pathway on global limonene-derived ON formation. O_3-initiated oxidation pathway of limonene is not included in Case2 while all the other settings are the same as Case0. The third sensitivity case (Case3) was designed to examine the effects of NO_3-initiated oxidation pathway on global limonene-derived ON formation, whose setup is referred to as the base case (Case0) excluding NO_3-initiated oxidation pathway of limonene. The fourth to sixth sensitivity case (Case4-6) was designed to examine the effects of individual initial oxidation pathway on global limonene-derived ON formation, whose setup is referred to as the base case (Case0) including OH, O_3 or NO_3-initiated oxidation pathway of limonene.

Section S3. Comparison With Measurements

The model's ability to simulate the formation of limonene-derived organonitrates (ON) is evaluated through comparisons with surface measurement data summarized in previous publication with references provided therein.(Li et al., 2023) Given that observational data do not differentiate ON formed specifically from limonene versus other VOC precursors, we compared simulated surface concentrations ON under two conditions, with and without developed limonene-derived ON formation mechanism in this study, against observations at 33 surface sites (Fig. S5). Global observation of ON concentration ranged from 0.1 to 6.1 $\mu g \cdot m^{-3}$. Simulations excluding limonene-derived ON formation largely underestimated the results by 92% (Table S10), which may be due to incomplete consideration of the precursors and formation process of ON in the mechanism. The incorporation of the limonene-derived ON formation mechanism improved global simulation of ON, resulting in increased simulated concentration of ON (0.05-0.50 $\mu g \cdot m^{-3}$) to achieve 85.2% lower than observations, especially at forest and coastal sites. The simulated ON concentration were within an order of magnitude of most particulate ON observations, though the simulated concentrations were still significantly lower than observed values in some urban and rural sites. It should be noted that this study primarily focused on developing explicit chemical mechanisms for global model to elucidate oxidation pathways of limonene from biogenic emission contributing to ON formation. The large underestimation at urban and suburban sites is likely due to the underestimation of ON generated from anthropogenic VOC emissions in this study, which is needed for further improvements in future research.

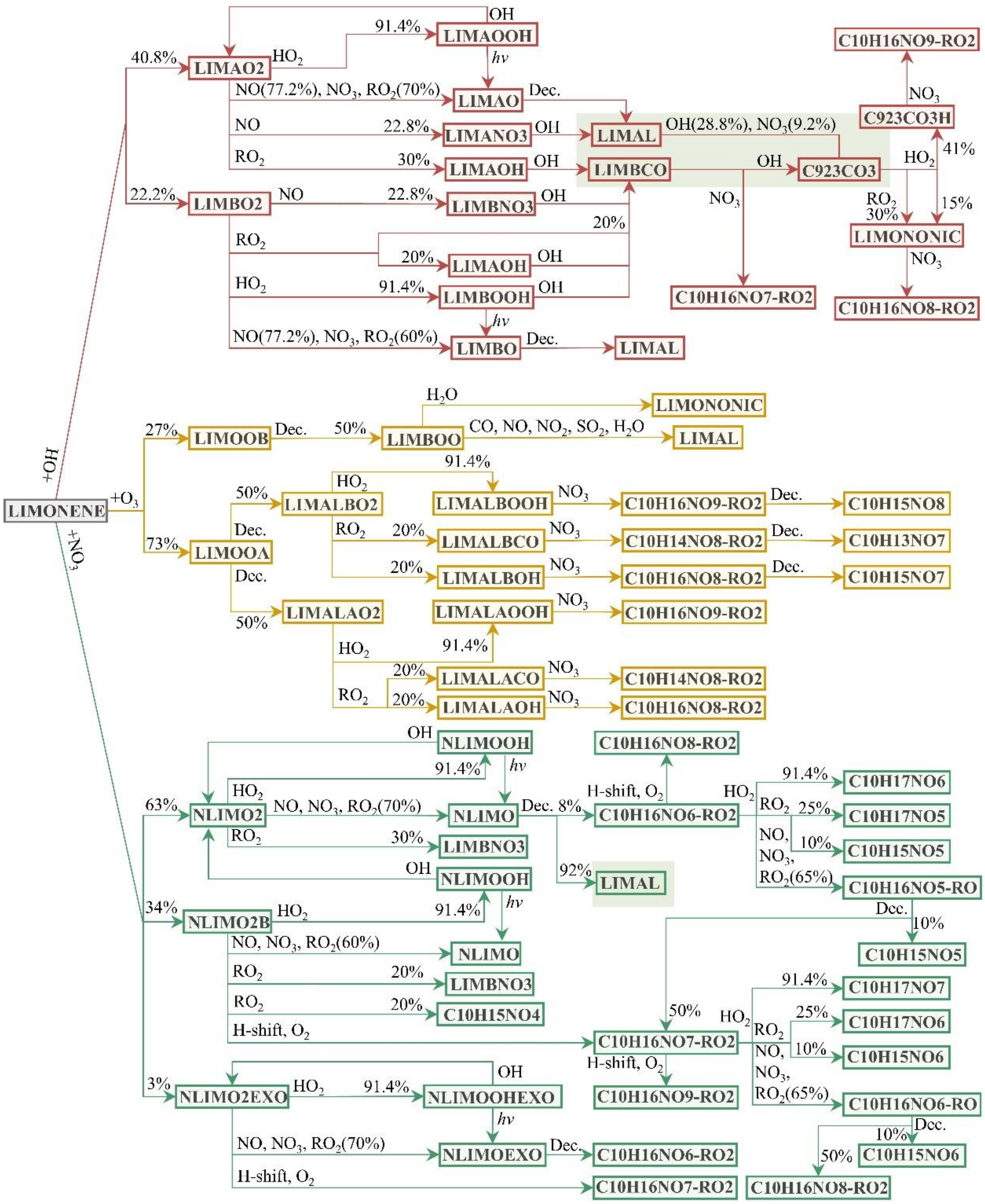

Figure S1. Limonene-derived ON gas-phase formation mechanism. If available, names of the species as they appear in Table S1 and MCM v3.3.1 are given. OH-initiated oxidation pathway of limonene is labeled in red; O_3-initiated oxidation pathway of limonene is labeled in yellow; NO_3-initiated oxidation pathway of limonene is labeled in green. Subsequent reactions with identical intermediates are represented only once. The green boxes indicate the intermediate oxidation pathways used for the experiments of NO_3-initiated oxidation pathways discussed in section 3.1.

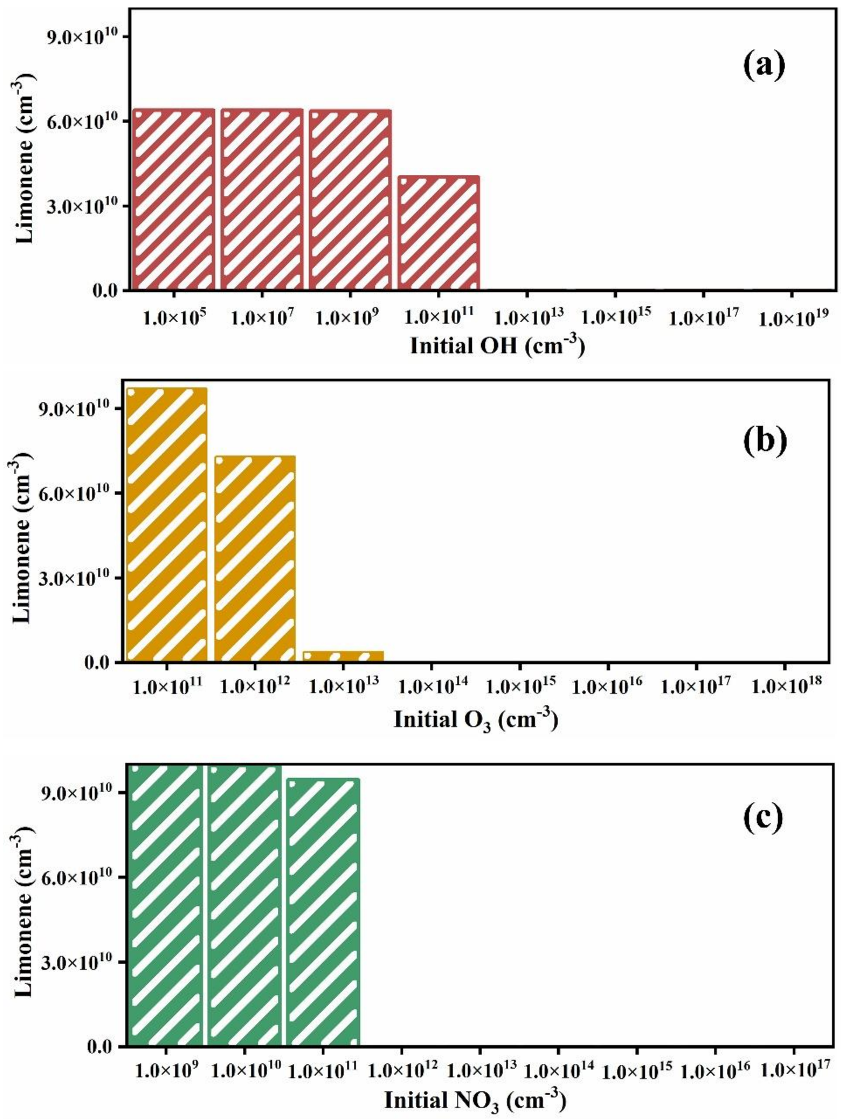

Figure S2. Simulated concentration variations of limonene from individual initial oxidation pathway under different (a) OH (red), (b) O_3 (yellow), (c) NO_3 (green) conditions using chemical box model.

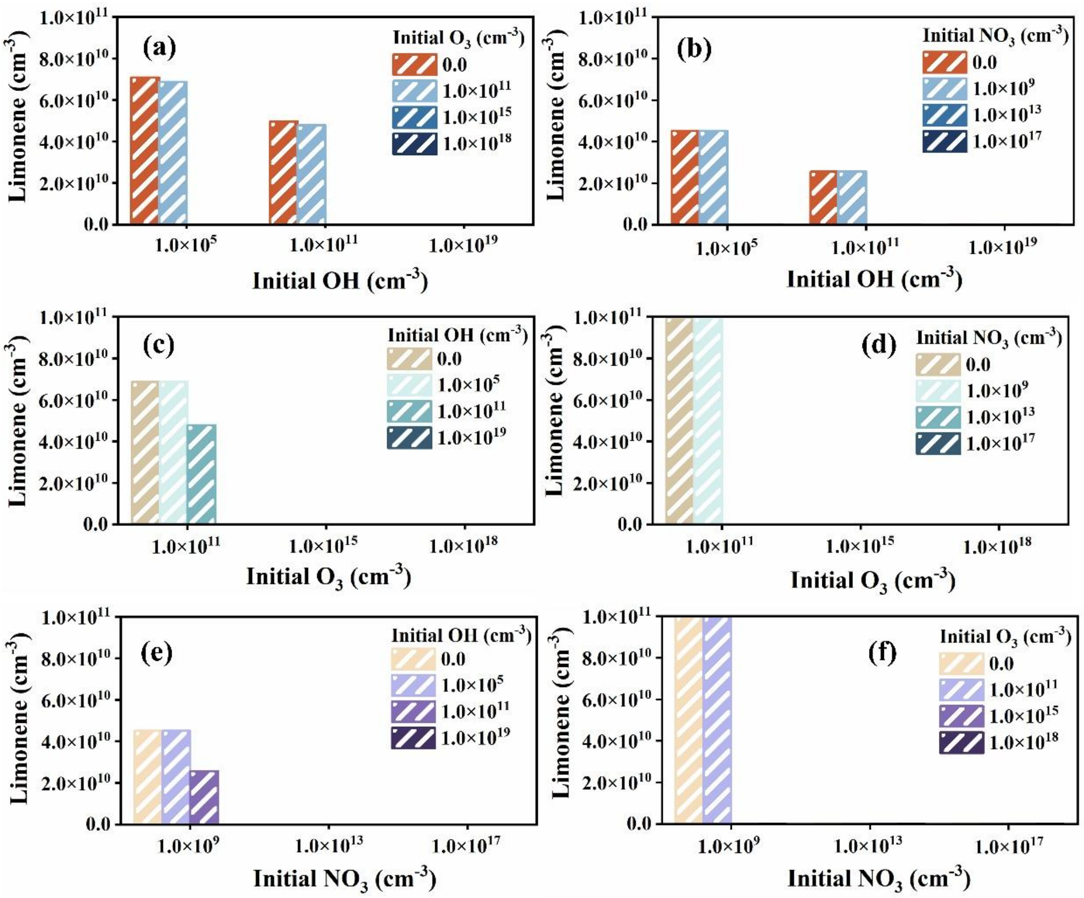

Figure S3. Simulated concentration variations of limonene by adding OH-initiated, O_3-initiated and NO_3-initiated oxidation pathways on the production of limonene-derived ON under different oxidant conditions, including variation of limonene concentration with adding initial OH concentration in the three O_3 levels under (a) low, (b) moderate and (c) high NO_3 levels; variation of limonene concentration with adding initial O_3 concentration in the three OH levels under (d) low, (e) moderate and (f) high NO_3 levels; variation of limonene concentration with adding initial NO_3 concentration in the three OH levels under (d) low, (e) moderate and (f) high O_3 levels.

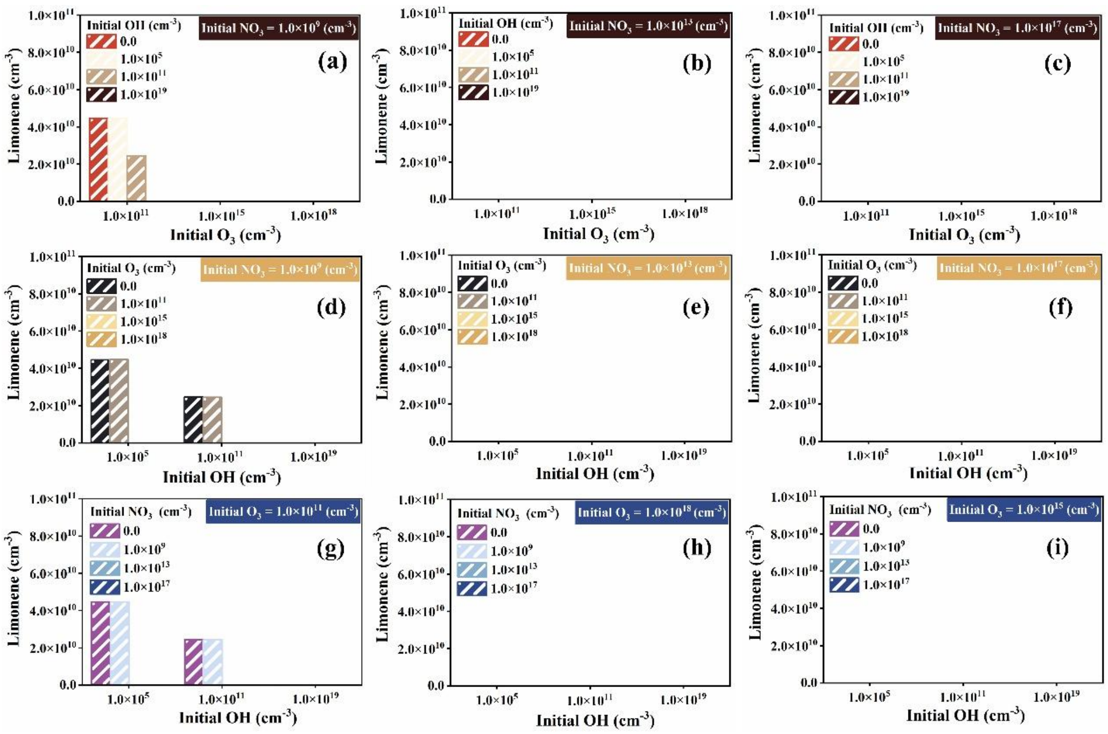

Figure S4. Simulated concentration variations of limonene by adding OH-, O_3- and NO_3-initiated oxidation pathways on the production of limonene-derived ON under different oxidant conditions, including variation of limonene concentration with adding initial OH concentration in the three O_3 levels under (a) low, (b) moderate and (c) high NO_3 levels; variation of limonene concentration with adding initial O_3 concentration in the three OH levels under (d) low, (e) moderate and (f) high NO_3 levels; variation of limonene concentration with adding initial NO_3 concentration in the three OH levels under (d) low, (e) moderate and (f) high O_3 levels.

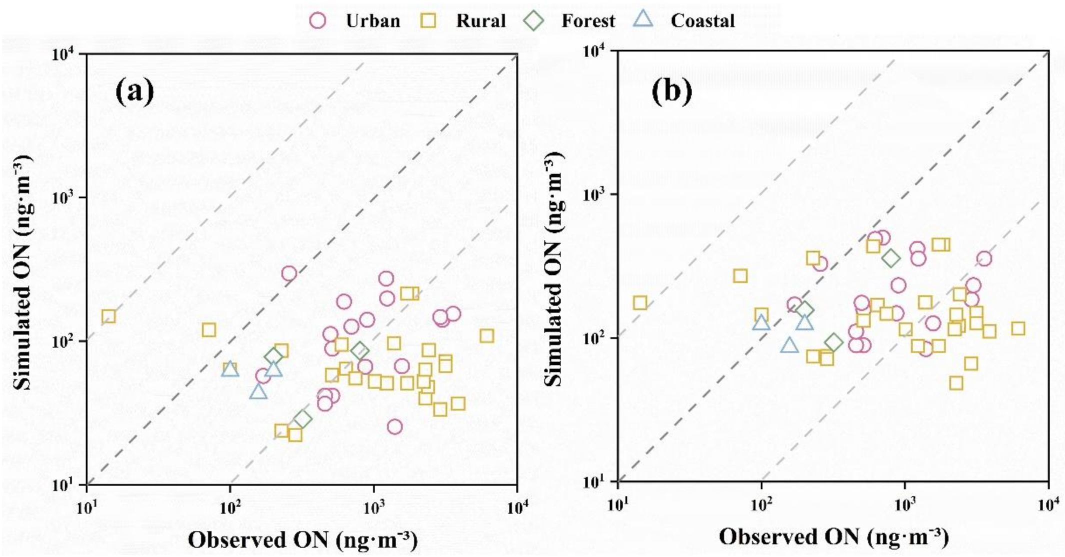

Figure S5. Simulated concentrations of ON and their comparisons against the total observed ON concentrations. (a) simulated ON without limonene-derived ON. (b) simulated ON including limonene-derived ON. Observations shown in colorful symbols: pink circles: urban sites; yellow square: rural sites; green diamond: forest sites; blue triangles: coastal sites. The dark grey dashed line indicates the 1:1 line; the light grey dashed lines indicate one order-of-magnitude differences. Details and references of the observations are shown in Table S9.

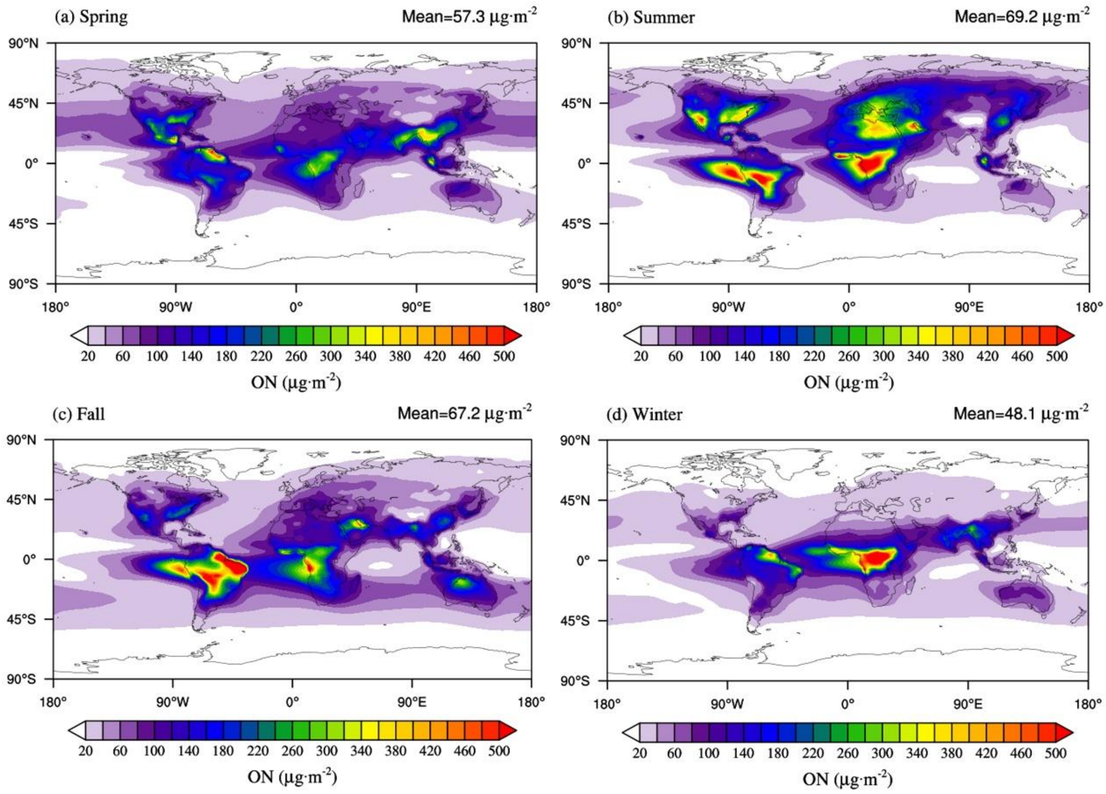

Figure S6. Simulated mean column concentration of limonene-derived ON (Case0) in spring (a), summer (b), fall (c), and winter (d).

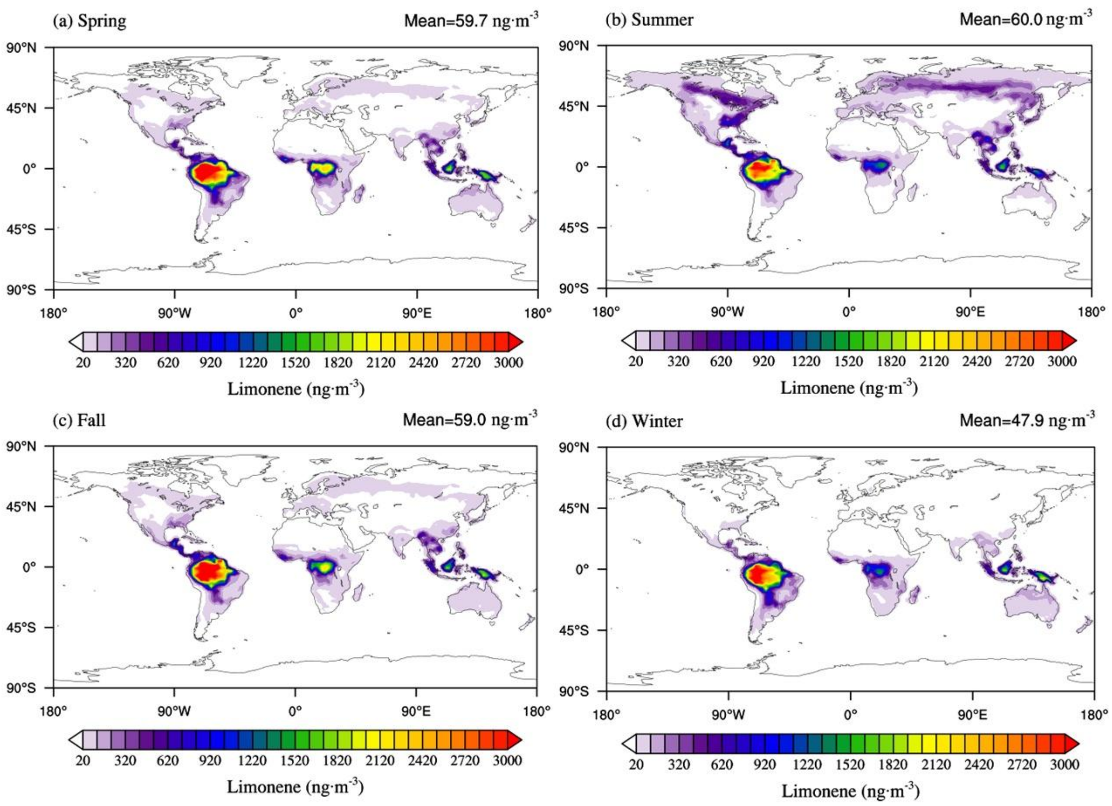

Figure S7. Simulated surface concentration of limonene (Case0) in spring (a), summer (b), fall (c), and winter (d).

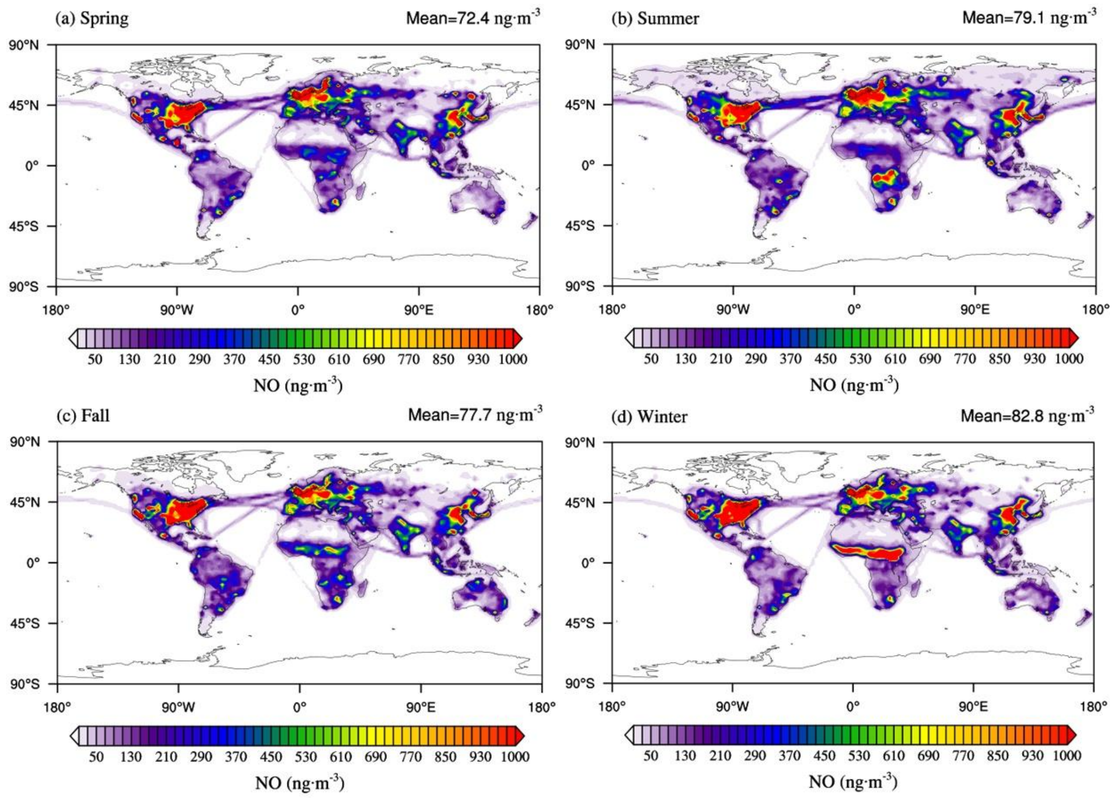

Figure S8. Simulated surface concentration of NO (Case0) in spring (a), summer (b), fall (c), and winter (d).

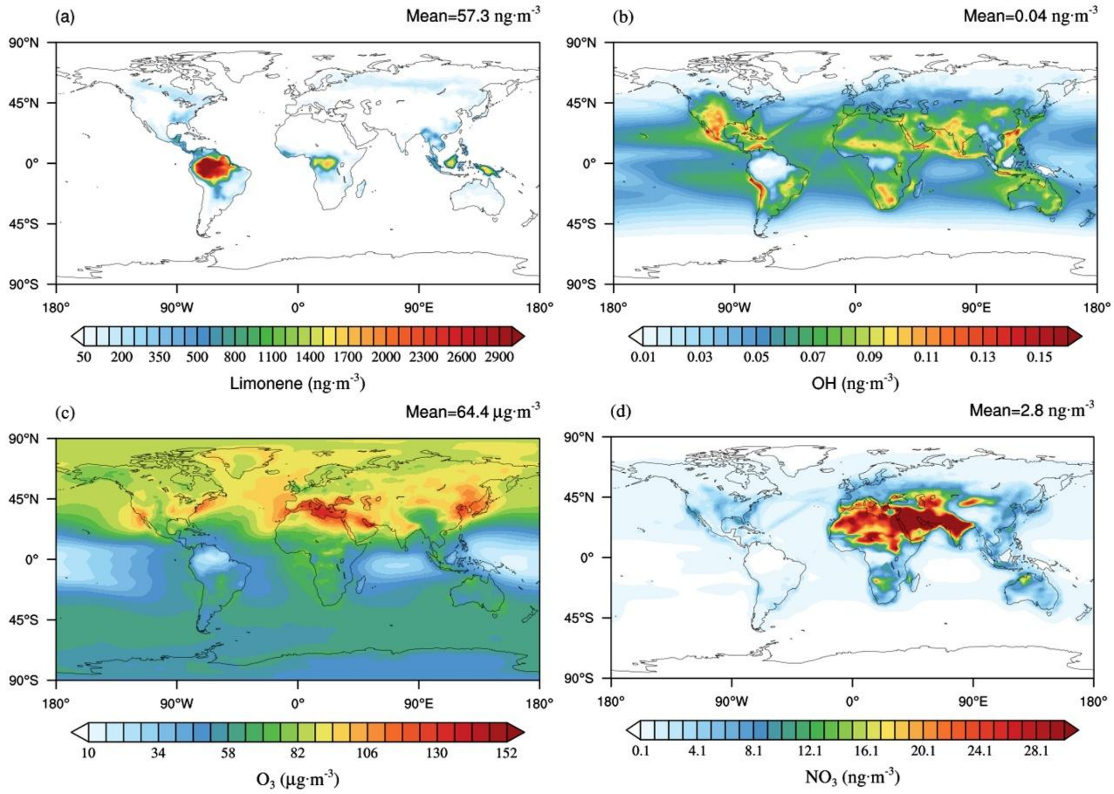

Figure S9. Simulated surface concentration of (a) limonene, (b) OH, (c) O_3 and (d) NO_3 for the Case0.

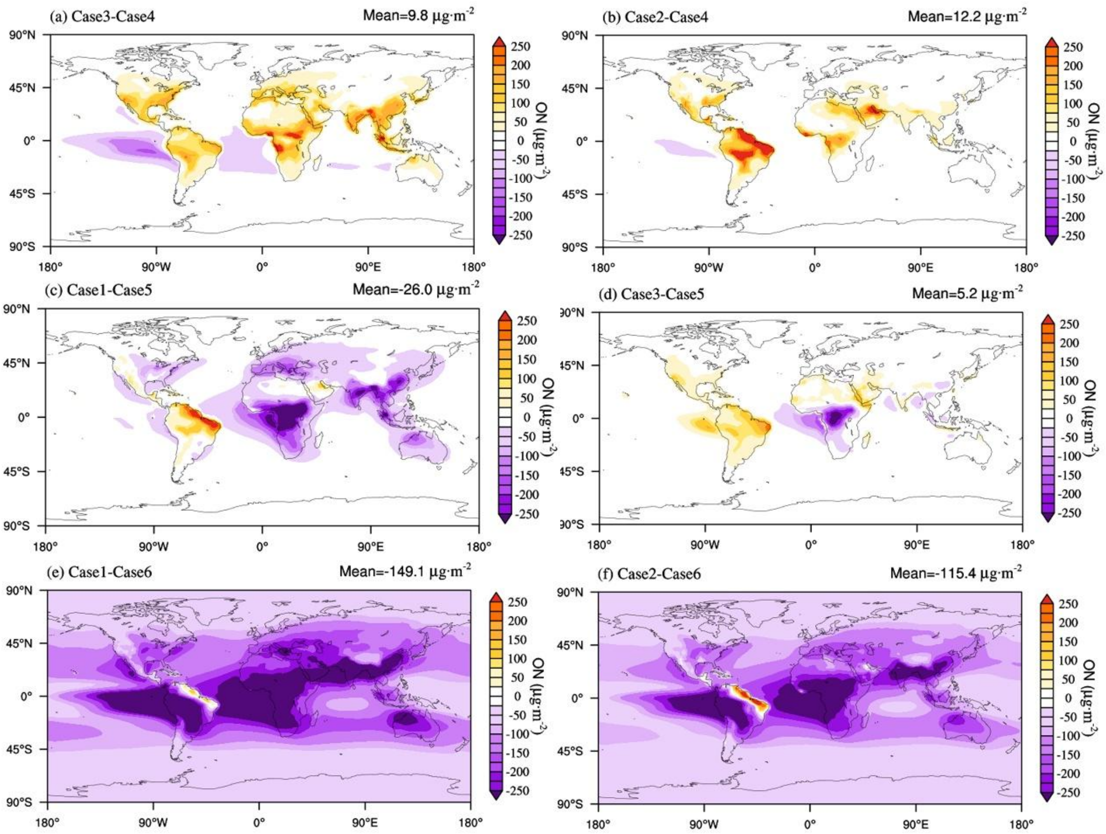

Figure S10. The difference in column concentration of limonene-derived ON between Case3 and Case4 (a), the difference in column concentration of limonene-derived ON between Case2 and Case4 (b), and the difference in column concentration of limonene-derived ON between Case1 and Case5 (c), the difference in column concentration of limonene-derived ON between Case3 and Case5 (d), the difference in column concentration of limonene-derived ON between Case1 and Case6 (e), the difference in column concentration of limonene-derived ON between Case2 and Case6 (f).

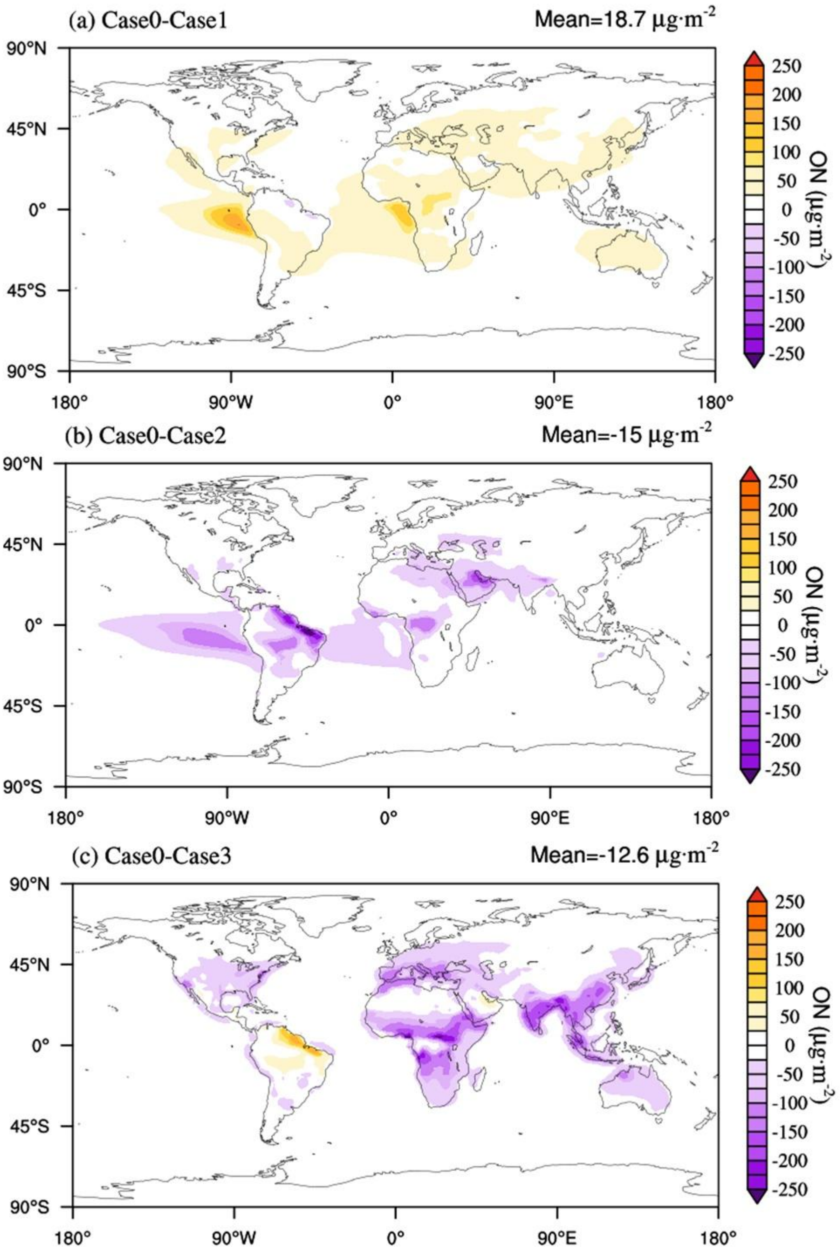

Figure S11. The difference in column concentration of limonene-derived ON between Case0 and Case1 (a), the difference in column concentration of limonene-derived ON between Case0 and Case2 (b), and the difference in column concentration of limonene-derived ON between Case0 and Case3 (c).

Table S1. Gas-phase species used in the limonene-derived ON formation mechanism

Short name	Chemical formula
LIMO	CH3C=CHCH2CH(CH2CH3)C(=CH2)CH2
LIMAO2	[O]OC(CH3)CH2CH2CH(CH2CHOH)C(=CH2)CH3
LIMBO2	[O]OCHCH2CH(CH2CH2C(CH3)OH)C(=CH2)CH3
LIMAOOH	HOOC(CH3)CH2CH2CH(CH2CHOH)C(=CH2)CH3
LIMBOOH	HOOCHCH2CH(CH2CH2C(CH3)OH)C(=CH2)CH3
LIMOOA	O=CHCH2CH(CH2CH2C(=[O+][O-])CH3)C(=CH2)CH3
LIMOOB	[O-][O+]=CHCH2CH(CH2CH2C(=O)CH3)C(=CH2)CH3
NLIMO2	[O-][N+](=O)OCHCH2CH(CH2CH2C(CH3)O[O])C(=CH2)CH3
NLIMO2B	[O]OCHCH2CH(CH2CH2C(CH3)O(=O)[N+][O-])C(=CH2)CH3
NLIMO2EXO	CH3C=CHCH2CH(CH2CH2)C(CH2O(=O)[N+][O-])(O[O])CH3
NLIMOOH	[O-][N+](=O)OCHCH2CH(CH2CH2C(CH3)OOH)C(=CH2)CH3
NLIMOOHEXO	CH3C=CHCH2CH(CH2CH2)C(CH2O(=O)[N+][O-])(OOH)CH3
LIMALAO2	O=CHCH2CH(CH2CH(O[O])C(=O)CH3)C(=CH2)CH3
LIMALBO2	[O]OCH2C(=O)CH2CH2CH(CH2CH=O)C(=CH2)CH3
LIMANO3	[O-][N+](=O)OC(CH3)CH2CH2CH(CH2CHOH)C(=CH2)CH3
LIMBNO3	[O-][N+](=O)OCHCH2CH(CH2CH2C(CH3)OH)C(=CH2)CH3
LIMALAOOH	O=CHCH2CH(CH2CH(OOH)C(=O)CH3)C(=CH2)CH3
LIMALBOOH	HOOCH2C(=O)CH2CH2CH(CH2CH=O)C(=CH2)CH3
C923CO3H	HOOC(=O)CH2CH(CH2CH2C(=O)CH3)C(=CH2)CH3
LIMBOO	[O-][O+]=CHCH2CH(CH2CH2C(=O)CH3)C(=CH2)CH3
LIMAO	CH3C(=CH2)CHCH2CH2C(CH3)([O])CH(OH)CH2
LIMBO	CH3C(=CH2)CHCH2CH2C(CH3)(OH)CH([O])CH2
NLIMO	[O-][N+](=O)OCHCH2CH(CH2CH2C(CH3)[O])C(=CH2)CH3
NLIMOEXO	CH3C=CHCH2CH(CH2CH2)C(CH2O(=O)[N+][O-])([O])CH3
LIMAL	O=CHCH2CH(CH2CH2C(=O)CH3)C(=CH2)CH3
LIMBCO	CH3C(=CH2)CHCH2CH2C(CH3)(OH)C(=O)CH2
LIMALACO	O=CHCH2CH(CH2C(=O)C(=O)CH3)C(=CH2)CH3
LIMALBCO	O=CHCH2CH(CH2CH2C(=O)CH=O)C(=CH2)CH3

Table S2. Reactions for limonene-derived ON formation mechanism.

Reaction	Rate constant (cm^3·molecules^{-1}·s^{-1} or s^{-1})	Note
LIMO + OH = LIMAO2	$4.3\times10^{-11}\times\exp(401/T)\times0.408$	b
LIMO + OH = LIMBO2	$4.3\times10^{-11}\times\exp(401/T)\times0.222$	b
LIMAO2 + HO2 = LIMAOOH	KRO2HO2×0.914	b
LIMAO2 + NO = LIMANO3	KRO2NO×0.228	b
LIMAO2 + NO = LIMAO + NO2	KRO2NO×0.772	b
LIMAO2 + NO3 = LIMAO + NO2	KRO2NO3	b
LIMAO2 + RO2 = LIMAO	$9.2\times10^{-14}\times0.7$	b
LIMAO2 + RO2 = LIMAOH	$9.2\times10^{-14}\times0.3$	b
LIMBO2 + HO2 = LIMBOOH	KRO2HO2×0.914	b
LIMBO2 + NO = LIMBNO3	KRO2NO×0.228	b
LIMBO2 + NO = LIMBO + NO2	KRO2NO×0.772	b
LIMBO2 + NO3 = LIMBO + NO2	KRO2NO3	b
LIMBO2 + RO2 = LIMBO	$8.8\times10^{-13}\times0.6$	b
LIMBO2 + RO2 = LIMAOH	$8.8\times10^{-13}\times0.2$	b
LIMBO2 + RO2 = LIMBCO	$8.8\times10^{-13}\times0.2$	b
LIMAOOH + OH = LIMAO2	7.4×10^{-11}	b
LIMAOOH + hv = LIMAO + OH	J<41>	b
LIMANO3 + OH = LIMAL + NO2	6.2×10^{-11}	b
LIMAO = LIMAL + HO2	KDEC	b
LIMAOH + OH = LIMBCO + HO2	7.0×10^{-11}	b
LIMBOOH + OH = LIMBCO + OH	1.0×10^{-10}	b
LIMBOOH + hv = LIMBO + OH	J<41>	b
LIMBNO3 + OH = LIMBCO + NO2	5.9×10^{-11}	b
LIMBO = LIMAL + HO2	KDEC	b
LIMO + O3 = LIMOOA	$2.8\times10^{-15}\times\exp(-770/T)\times0.73$	b
LIMO + O3 = LIMOOB	$2.8\times10^{-15}\times\exp(-770/T)\times0.27$	b
LIMOOA = LIMALAO2 + OH	KDEC×0.5	b
LIMOOA = LIMALBO2 + OH	KDEC×0.5	b
LIMOOB = LIMBOO	KDEC×0.5	b
LIMALAO2 + HO2 = LIMALAOOH	KRO2HO2×0.914	b
LIMALAO2 + RO2= LIMALACO	$8.8\times10^{-13}\times0.2$	b
LIMALAO2 + RO2 = LIMALAOH	$8.8\times10^{-13}\times0.2$	b

LIMALBO2 + HO2 = LIMALBOOH	KRO2HO2×0.914	b
LIMALBO2 + RO2= LIMALBCO	$8.8\times10^{-13}\times0.05$	b
LIMALBO2 + RO2 = LIMALBOH	$8.8\times10^{-13}\times0.05$	b
LIMBOO + CO = LIMAL	1.2×10^{-15}	b
LIMBOO + NO = LIMAL	1.0×10^{-14}	b
LIMBOO + NO2 = LIMAL	1.0×10^{-15}	b
LIMBOO + SO2 = LIMAL + SO3	7.0×10^{-14}	b
LIMBOO + H2O = LIMAL + H2O2	1.4×10^{-17}	b
LIMBOO + H2O = LIMNONIC	2.0×10^{-18}	b
LIMO + NO3 = NLIMO2	$1.2\times10^{-11}\times0.63$	b
LIMO + NO3 = NLIMO2B	$1.2\times10^{-11}\times0.34$	b
LIMO + NO3 = NLIMO2EXO	$1.2\times10^{-11}\times0.03$	b
NLIMO2 + HO2 = NLIMOOH	KRO2HO2×0.914	b
NLIMO2 + NO = NLIMO + NO2	KRO2NO	b
NLIMO2 + NO3 = NLIMO + NO2	KRO2NO3	b
NLIMO2 + RO2 => LIMBNO3	$9.2\times10^{-14}\times0.3$	b
NLIMO2 + RO2 = NLIMO	$9.2\times10^{-14}\times0.7$	b
NLIMO2B + HO2 = NLIMOOH	KRO2HO2×0.914	a,b
NLIMO2B + NO = NLIMO + NO2	KRO2NO	a,b
NLIMO2B + NO3 = NLIMO + NO2	KRO2NO3	a,b
NLIMO2B + RO2 = LIMBNO3	$8.8\times10^{-13}\times0.2$	a,b
NLIMO2B + RO2 = C10H15NO4	$8.8\times10^{-13}\times0.2$	a,b
NLIMO2B + RO2 = NLIMO	$8.8\times10^{-13}\times0.6$	a,b
NLIMO2B = C10H16NO7RO2	0.02	a,b
NLIMO2EXO + HO2 = NLIMOOHEXO	KRO2HO2×0.914	a,b
NLIMO2EXO + NO = NLIMOEXO + NO2	KRO2NO	a,b
NLIMO2EXO + NO3 = NLIMOEXO + NO2	KRO2NO3	a,b
NLIMO2EXO + RO2 = NLIMOEXO	$9.2\times10^{-14}\times0.7$	a,b
NLIMO2EXO = C10H16NO7RO2	20	a,c
NLIMOEXO = C10H16NO6RO2	KDEC×0.5	a,b,d
NLIMOOH + OH = NLIMO2	4.3×10^{-11}	a,b
NLIMOOH + hv = NLIMO + OH	J<41>	a,b
NLIMOOHEXO + OH = NLIMO2EXO	4.3×10^{-11}	a,b
NLIMOOHEXO + hv = NLIMOEXO + OH	J<41>	a,b
NLIMO = LIMAL + NO2	KDEC×0.92	b

NLIMO = C10H16NO6RO2	KDEC×0.08	b
LIMAL + NO3 = C923CO3 + HNO3	$1.1\times10^{-10}\times0.092$	b
LIMAL + OH = C923CO3	$1.1\times10^{-10}\times0.288$	b
LIMBCO + OH = C923CO3	6.7×10^{-11}	b
LIMBCO + NO3 = C10H16NO7RO2	2.6×10^{-13}	b
C923CO3 + HO2 = C923CO3H	KAPHO2×0.41	b
C923CO3 + HO2 = LIMNONIC + O3	KAPHO2×0.15	b
C923CO3 + RO2 = LIMNONIC	$1.0\times10^{-10}\times0.3$	b
C923CO3H + NO3 = C10H16NO9RO2	2.6×10^{-13}	b
LIMNONIC + NO3 = C10H16NO8RO2	2.6×10^{-13}	b
LIMALAOH + NO3 = C10H16NO8RO2	2.6×10^{-13}	b
LIMALACO + NO3 => C10H14NO8RO2	2.6×10^{-13}	b
LIMALAOOH + NO3 = C10H16NO9RO2	2.6×10^{-13}	b
LIMALBOH + NO3 = C10H16NO8RO2	2.6×10^{-13}	b
LIMALBCO + NO3 => C10H14NO8RO2	2.6×10^{-13}	b
LIMALBOOH + NO3 = C10H16NO9RO2	2.6×10^{-13}	b
C10H16NO6RO2 + HO2 = C10H17NO6	KRO2HO2×0.914	b
C10H16NO6RO2 + NO = C10H16NO5RO + NO2	KRO2NO	b
C10H16NO6RO2 + NO3 = C10H16NO5RO + NO2	KRO2NO3	b
C10H16NO6RO2 + RO2 = C10H17NO5	$5.0\times10^{-13}\times0.25$	c
C10H16NO6RO2 + RO2 = C10H15NO5	$5.0\times10^{-13}\times0.1$	c
C10H16NO6RO2 + RO2 = C10H16NO5RO	$5.0\times10^{-13}\times0.65$	c
C10H16NO6RO2 = C10H16NO8RO2	0.2	c
C10H16NO8RO2 = C10H15NO7 + OH	0.1	c
C10H16NO5RO = C10H15NO5 + HO2	KDEC×0.1	b,d
C10H16NO5RO = C10H16NO7RO2	KDEC×0.5	b,d
C10H16NO7RO2 + HO2 = C10H17NO7	KRO2HO2×0.914	b
C10H16NO7RO2 + NO = C10H16NO6RO + NO2	KRO2NO	b
C10H16NO7RO2 + NO3 = C10H16NO6RO + NO2	KRO2NO3	b
C10H16NO7RO2 + RO2 = C10H17NO6	$5.0\times10^{-13}\times0.25$	c
C10H16NO7RO2 + RO2 = C10H15NO6	$5.0\times10^{-13}\times0.1$	c
C10H16NO7RO2 + RO2 = C10H16NO6RO	$5.0\times10^{-13}\times0.65$	c
C10H16NO7RO2 = C10H16NO9RO2	0.2	c
C10H16NO6RO = C10H15NO6 + HO2	KDEC×0.1	b,d
C10H16NO6RO = C10H16NO8RO2	KDEC×0.5	b,d

C10H16NO9RO2 = C10H15NO8 + OH	0.1	c
C10H14NO8RO2 = C10H13NO7 + OH	0.1	c

[a]New short names are given for species not existing in MCM. [b]Rate constants refer to Master Chemical Mechanism (MCM). [c]Rate constants refer to recent studies (Mayorga et al., 2022). [d]The branching ratios are estimated from recent studies (Mayorga et al., 2022).

Table S3. Summary of vapor pressures of highly oxygenated limonene-derived ON calculated by two methods under standard conditions (298 K).

Species	Vapor pressure (atm)	
	EVAPORATION	SIMPOL
$C_{10}H_{13}NO_7$	1.4×10^{-7}	1.7×10^{-7}
$C_{10}H_{15}NO_4$	1.1×10^{-6}	1.7×10^{-6}
$C_{10}H_{15}NO_5$	2.7×10^{-7}	6.2×10^{-8}
$C_{10}H_{15}NO_6$	3.5×10^{-8}	2.7×10^{-8}
$C_{10}H_{15}NO_7$	2.3×10^{-8}	5.5×10^{-8}
$C_{10}H_{15}NO_8$	7.9×10^{-10}	3.6×10^{-10}
$C_{10}H_{17}NO_5$	1.5×10^{-8}	4.8×10^{-8}
$C_{10}H_{17}NO_6$	6.6×10^{-9}	8.4×10^{-9}
$C_{10}H_{17}NO_7$	2.6×10^{-9}	3.3×10^{-8}

Table S4. Compilation of experiments in chemical box model.

Scheme	Initial concentration of species (cm^{-3})									Description
	LIMO	OH	O_3	NO_3	NO	CO	SO_2	HO_2	H_2O	
OH	1.0×10^{11}	1.0×10^{5}~1.0×10^{19}	0.0	1.0×10^{12}	1.0×10^{12}	0.0	0.0	1.0×10^{11}	0.0	Limonene-derived ON formation under individual initial oxidation pathway
O_3	1.0×10^{11}	1.0×10^{10}	1.0×10^{11}~1.0×10^{18}	1.0×10^{12}	1.0×10^{12}	1.0×10^{14}	1.0×10^{10}	1.0×10^{11}	1.0×10^{16}	
NO_3	1.0×10^{11}	1.0×10^{10}	0.0	1.0×10^{9}~1.0×10^{17}	1.0×10^{12}	0.0	0.0	1.0×10^{11}	0.0	
OH+O_3	1.0×10^{11}	0.0/1.0×10^{5}/1.0×10^{11}/1.0×10^{19}	0.0/1.0×10^{11}/1.0×10^{15}/1.0×10^{18}	1.0×10^{12}	1.0×10^{12}	1.0×10^{14}	1.0×10^{10}	1.0×10^{11}	1.0×10^{16}	Limonene-derived ON formation under multiple initial oxidation pathways
OH+NO_3	1.0×10^{11}	0.0/1.0×10^{5}/1.0×10^{11}/1.0×10^{19}	0.0	0.0/1.0×10^{9}/1.0×10^{13}/1.0×10^{17}	1.0×10^{12}	0.0	0.0	1.0×10^{11}	0.0	
O_3+NO_3	1.0×10^{11}	1.0×10^{10}	0.0/1.0×10^{11}/1.0×10^{15}/1.0×10^{18}	0.0/1.0×10^{9}/1.0×10^{13}/1.0×10^{17}	1.0×10^{12}	1.0×10^{14}	1.0×10^{10}	1.0×10^{11}	1.0×10^{16}	
OH+O_3+NO_3	1.0×10^{11}	0.0/1.0×10^{5}/1.0×10^{11}/1.0×10^{19}	0.0/1.0×10^{11}/1.0×10^{15}/1.0×10^{18}	0.0/1.0×10^{9}/1.0×10^{13}/1.0×10^{17}	1.0×10^{12}	1.0×10^{14}	1.0×10^{10}	1.0×10^{11}	1.0×10^{16}	

Table S5. Initial concentrations of species used in chemical box model experiments.

Scheme	Species (cm^{-3})								
	LIMO	OH	O_3	NO_3	NO	CO	SO_2	HO_2	H_2O
OH	1.0×10^{11}	1.0×10^{5}	0.0	1.0×10^{12}	1.0×10^{12}	0.0	0.0	1.0×10^{11}	0.0
	1.0×10^{11}	1.0×10^{7}	0.0	1.0×10^{12}	1.0×10^{12}	0.0	0.0	1.0×10^{11}	0.0
	1.0×10^{11}	1.0×10^{9}	0.0	1.0×10^{12}	1.0×10^{12}	0.0	0.0	1.0×10^{11}	0.0
	1.0×10^{11}	1.0×10^{11}	0.0	1.0×10^{12}	1.0×10^{12}	0.0	0.0	1.0×10^{11}	0.0
	1.0×10^{11}	1.0×10^{13}	0.0	1.0×10^{12}	1.0×10^{12}	0.0	0.0	1.0×10^{11}	0.0
	1.0×10^{11}	1.0×10^{15}	0.0	1.0×10^{12}	1.0×10^{12}	0.0	0.0	1.0×10^{11}	0.0
	1.0×10^{11}	1.0×10^{17}	0.0	1.0×10^{12}	1.0×10^{12}	0.0	0.0	1.0×10^{11}	0.0
	1.0×10^{11}	1.0×10^{19}	0.0	1.0×10^{12}	1.0×10^{12}	0.0	0.0	1.0×10^{11}	0.0
O_3	1.0×10^{11}	1.0×10^{10}	1.0×10^{11}	1.0×10^{12}	1.0×10^{12}	1.0×10^{14}	1.0×10^{10}	1.0×10^{11}	1.0×10^{16}
	1.0×10^{11}	1.0×10^{10}	1.0×10^{12}	1.0×10^{12}	1.0×10^{12}	1.0×10^{14}	1.0×10^{10}	1.0×10^{11}	1.0×10^{16}
	1.0×10^{11}	1.0×10^{10}	1.0×10^{13}	1.0×10^{12}	1.0×10^{12}	1.0×10^{14}	1.0×10^{10}	1.0×10^{11}	1.0×10^{16}
	1.0×10^{11}	1.0×10^{10}	1.0×10^{14}	1.0×10^{12}	1.0×10^{12}	1.0×10^{14}	1.0×10^{10}	1.0×10^{11}	1.0×10^{16}
	1.0×10^{11}	1.0×10^{10}	1.0×10^{15}	1.0×10^{12}	1.0×10^{12}	1.0×10^{14}	1.0×10^{10}	1.0×10^{11}	1.0×10^{16}
	1.0×10^{11}	1.0×10^{10}	1.0×10^{16}	1.0×10^{12}	1.0×10^{12}	1.0×10^{14}	1.0×10^{10}	1.0×10^{11}	1.0×10^{16}
	1.0×10^{11}	1.0×10^{10}	1.0×10^{17}	1.0×10^{12}	1.0×10^{12}	1.0×10^{14}	1.0×10^{10}	1.0×10^{11}	1.0×10^{16}
	1.0×10^{11}	1.0×10^{10}	1.0×10^{18}	1.0×10^{12}	1.0×10^{12}	1.0×10^{14}	1.0×10^{10}	1.0×10^{11}	1.0×10^{16}
NO_3	1.0×10^{11}	1.0×10^{10}	0.0	1.0×10^{9}	1.0×10^{12}	0.0	0.0	1.0×10^{11}	0.0
	1.0×10^{11}	1.0×10^{10}	0.0	1.0×10^{10}	1.0×10^{12}	0.0	0.0	1.0×10^{11}	0.0
	1.0×10^{11}	1.0×10^{10}	0.0	1.0×10^{11}	1.0×10^{12}	0.0	0.0	1.0×10^{11}	0.0
	1.0×10^{11}	1.0×10^{10}	0.0	1.0×10^{12}	1.0×10^{12}	0.0	0.0	1.0×10^{11}	0.0
	1.0×10^{11}	1.0×10^{10}	0.0	1.0×10^{13}	1.0×10^{12}	0.0	0.0	1.0×10^{11}	0.0
	1.0×10^{11}	1.0×10^{10}	0.0	1.0×10^{14}	1.0×10^{12}	0.0	0.0	1.0×10^{11}	0.0
	1.0×10^{11}	1.0×10^{10}	0.0	1.0×10^{15}	1.0×10^{12}	0.0	0.0	1.0×10^{11}	0.0
	1.0×10^{11}	1.0×10^{10}	0.0	1.0×10^{16}	1.0×10^{12}	0.0	0.0	1.0×10^{11}	0.0
	1.0×10^{11}	1.0×10^{10}	0.0	1.0×10^{17}	1.0×10^{12}	0.0	0.0	1.0×10^{11}	0.0
OH + O_3	1.0×10^{11}	1.0×10^{5}	0.0	1.0×10^{12}	1.0×10^{12}	1.0×10^{14}	1.0×10^{10}	1.0×10^{11}	1.0×10^{16}
	1.0×10^{11}	1.0×10^{11}	0.0	1.0×10^{12}	1.0×10^{12}	1.0×10^{14}	1.0×10^{10}	1.0×10^{11}	1.0×10^{16}

	1.0×10^{11}	1.0×10^{19}	0.0	1.0×10^{12}	1.0×10^{12}	1.0×10^{14}	1.0×10^{10}	1.0×10^{11}	1.0×10^{16}
	1.0×10^{11}	0.0	1.0×10^{11}	1.0×10^{12}	1.0×10^{12}	1.0×10^{14}	1.0×10^{10}	1.0×10^{11}	1.0×10^{16}
	1.0×10^{11}	0.0	1.0×10^{15}	1.0×10^{12}	1.0×10^{12}	1.0×10^{14}	1.0×10^{10}	1.0×10^{11}	1.0×10^{16}
	1.0×10^{11}	0.0	1.0×10^{18}	1.0×10^{12}	1.0×10^{12}	1.0×10^{14}	1.0×10^{10}	1.0×10^{11}	1.0×10^{16}
	1.0×10^{11}	1.0×10^{5}	1.0×10^{11}	1.0×10^{12}	1.0×10^{12}	1.0×10^{14}	1.0×10^{10}	1.0×10^{11}	1.0×10^{16}
	1.0×10^{11}	1.0×10^{5}	1.0×10^{15}	1.0×10^{12}	1.0×10^{12}	1.0×10^{14}	1.0×10^{10}	1.0×10^{11}	1.0×10^{16}
	1.0×10^{11}	1.0×10^{5}	1.0×10^{18}	1.0×10^{12}	1.0×10^{12}	1.0×10^{14}	1.0×10^{10}	1.0×10^{11}	1.0×10^{16}
	1.0×10^{11}	1.0×10^{11}	1.0×10^{11}	1.0×10^{12}	1.0×10^{12}	1.0×10^{14}	1.0×10^{10}	1.0×10^{11}	1.0×10^{16}
	1.0×10^{11}	1.0×10^{11}	1.0×10^{15}	1.0×10^{12}	1.0×10^{12}	1.0×10^{14}	1.0×10^{10}	1.0×10^{11}	1.0×10^{16}
	1.0×10^{11}	1.0×10^{11}	1.0×10^{18}	1.0×10^{12}	1.0×10^{12}	1.0×10^{14}	1.0×10^{10}	1.0×10^{11}	1.0×10^{16}
	1.0×10^{11}	1.0×10^{19}	1.0×10^{11}	1.0×10^{12}	1.0×10^{12}	1.0×10^{14}	1.0×10^{10}	1.0×10^{11}	1.0×10^{16}
	1.0×10^{11}	1.0×10^{19}	1.0×10^{15}	1.0×10^{12}	1.0×10^{12}	1.0×10^{14}	1.0×10^{10}	1.0×10^{11}	1.0×10^{16}
	1.0×10^{11}	1.0×10^{19}	1.0×10^{18}	1.0×10^{12}	1.0×10^{12}	1.0×10^{14}	1.0×10^{10}	1.0×10^{11}	1.0×10^{16}
$OH + NO_3$	1.0×10^{11}	0.0	0.0	1.0×10^{9}	1.0×10^{12}	0.0	0.0	1.0×10^{11}	0.0
	1.0×10^{11}	0.0	0.0	1.0×10^{13}	1.0×10^{12}	0.0	0.0	1.0×10^{11}	0.0
	1.0×10^{11}	0.0	0.0	1.0×10^{17}	1.0×10^{12}	0.0	0.0	1.0×10^{11}	0.0
	1.0×10^{11}	1.0×10^{5}	0.0	0.0	1.0×10^{12}	0.0	0.0	1.0×10^{11}	0.0
	1.0×10^{11}	1.0×10^{11}	0.0	0.0	1.0×10^{12}	0.0	0.0	1.0×10^{11}	0.0
	1.0×10^{11}	1.0×10^{19}	0.0	0.0	1.0×10^{12}	0.0	0.0	1.0×10^{11}	0.0
	1.0×10^{11}	1.0×10^{5}	0.0	1.0×10^{9}	1.0×10^{12}	0.0	0.0	1.0×10^{11}	0.0
	1.0×10^{11}	1.0×10^{5}	0.0	1.0×10^{13}	1.0×10^{12}	0.0	0.0	1.0×10^{11}	0.0
	1.0×10^{11}	1.0×10^{5}	0.0	1.0×10^{17}	1.0×10^{12}	0.0	0.0	1.0×10^{11}	0.0
	1.0×10^{11}	1.0×10^{11}	0.0	1.0×10^{9}	1.0×10^{12}	0.0	0.0	1.0×10^{11}	0.0
	1.0×10^{11}	1.0×10^{11}	0.0	1.0×10^{13}	1.0×10^{12}	0.0	0.0	1.0×10^{11}	0.0
	1.0×10^{11}	1.0×10^{11}	0.0	1.0×10^{17}	1.0×10^{12}	0.0	0.0	1.0×10^{11}	0.0
	1.0×10^{11}	1.0×10^{19}	0.0	1.0×10^{9}	1.0×10^{12}	0.0	0.0	1.0×10^{11}	0.0
	1.0×10^{11}	1.0×10^{19}	0.0	1.0×10^{13}	1.0×10^{12}	0.0	0.0	1.0×10^{11}	0.0
	1.0×10^{11}	1.0×10^{19}	0.0	1.0×10^{17}	1.0×10^{12}	0.0	0.0	1.0×10^{11}	0.0
$O_3 + NO_3$	1.0×10^{11}	1.0×10^{10}	1.0×10^{11}	0.0	1.0×10^{12}	1.0×10^{14}	1.0×10^{10}	1.0×10^{11}	1.0×10^{16}
	1.0×10^{11}	1.0×10^{10}	1.0×10^{15}	0.0	1.0×10^{12}	1.0×10^{14}	1.0×10^{10}	1.0×10^{11}	1.0×10^{16}

	1.0×10^{11}	1.0×10^{10}	1.0×10^{18}	0.0	1.0×10^{12}	1.0×10^{14}	1.0×10^{10}	1.0×10^{11}	1.0×10^{16}
	1.0×10^{11}	1.0×10^{10}	0.0	1.0×10^{9}	1.0×10^{12}	1.0×10^{14}	1.0×10^{10}	1.0×10^{11}	1.0×10^{16}
	1.0×10^{11}	1.0×10^{10}	0.0	1.0×10^{13}	1.0×10^{12}	1.0×10^{14}	1.0×10^{10}	1.0×10^{11}	1.0×10^{16}
	1.0×10^{11}	1.0×10^{10}	0.0	1.0×10^{17}	1.0×10^{12}	1.0×10^{14}	1.0×10^{10}	1.0×10^{11}	1.0×10^{16}
	1.0×10^{11}	1.0×10^{10}	1.0×10^{11}	1.0×10^{9}	1.0×10^{12}	1.0×10^{14}	1.0×10^{10}	1.0×10^{11}	1.0×10^{16}
	1.0×10^{11}	1.0×10^{10}	1.0×10^{11}	1.0×10^{13}	1.0×10^{12}	1.0×10^{14}	1.0×10^{10}	1.0×10^{11}	1.0×10^{16}
	1.0×10^{11}	1.0×10^{10}	1.0×10^{11}	1.0×10^{17}	1.0×10^{12}	1.0×10^{14}	1.0×10^{10}	1.0×10^{11}	1.0×10^{16}
	1.0×10^{11}	1.0×10^{10}	1.0×10^{15}	1.0×10^{9}	1.0×10^{12}	1.0×10^{14}	1.0×10^{10}	1.0×10^{11}	1.0×10^{16}
	1.0×10^{11}	1.0×10^{10}	1.0×10^{15}	1.0×10^{13}	1.0×10^{12}	1.0×10^{14}	1.0×10^{10}	1.0×10^{11}	1.0×10^{16}
	1.0×10^{11}	1.0×10^{10}	1.0×10^{15}	1.0×10^{17}	1.0×10^{12}	1.0×10^{14}	1.0×10^{10}	1.0×10^{11}	1.0×10^{16}
	1.0×10^{11}	1.0×10^{10}	1.0×10^{18}	1.0×10^{9}	1.0×10^{12}	1.0×10^{14}	1.0×10^{10}	1.0×10^{11}	1.0×10^{16}
	1.0×10^{11}	1.0×10^{10}	1.0×10^{18}	1.0×10^{13}	1.0×10^{12}	1.0×10^{14}	1.0×10^{10}	1.0×10^{11}	1.0×10^{16}
	1.0×10^{11}	1.0×10^{10}	1.0×10^{18}	1.0×10^{17}	1.0×10^{12}	1.0×10^{14}	1.0×10^{10}	1.0×10^{11}	1.0×10^{16}
$OH + O_3 + NO_3$	1.0×10^{11}	1.0×10^{5}	0.0	1.0×10^{9}	1.0×10^{12}	1.0×10^{14}	1.0×10^{10}	1.0×10^{11}	1.0×10^{16}
	1.0×10^{11}	1.0×10^{5}	0.0	1.0×10^{13}	1.0×10^{12}	1.0×10^{14}	1.0×10^{10}	1.0×10^{11}	1.0×10^{16}
	1.0×10^{11}	1.0×10^{5}	0.0	1.0×10^{17}	1.0×10^{12}	1.0×10^{14}	1.0×10^{10}	1.0×10^{11}	1.0×10^{16}
	1.0×10^{11}	1.0×10^{11}	0.0	1.0×10^{9}	1.0×10^{12}	1.0×10^{14}	1.0×10^{10}	1.0×10^{11}	1.0×10^{16}
	1.0×10^{11}	1.0×10^{11}	0.0	1.0×10^{13}	1.0×10^{12}	1.0×10^{14}	1.0×10^{10}	1.0×10^{11}	1.0×10^{16}
	1.0×10^{11}	1.0×10^{11}	0.0	1.0×10^{17}	1.0×10^{12}	1.0×10^{14}	1.0×10^{10}	1.0×10^{11}	1.0×10^{16}
	1.0×10^{11}	1.0×10^{19}	0.0	1.0×10^{9}	1.0×10^{12}	1.0×10^{14}	1.0×10^{10}	1.0×10^{11}	1.0×10^{16}
	1.0×10^{11}	1.0×10^{19}	0.0	1.0×10^{13}	1.0×10^{12}	1.0×10^{14}	1.0×10^{10}	1.0×10^{11}	1.0×10^{16}
	1.0×10^{11}	1.0×10^{19}	0.0	1.0×10^{17}	1.0×10^{12}	1.0×10^{14}	1.0×10^{10}	1.0×10^{11}	1.0×10^{16}
	1.0×10^{11}	1.0×10^{5}	1.0×10^{11}	0.0	1.0×10^{12}	1.0×10^{14}	1.0×10^{10}	1.0×10^{11}	1.0×10^{16}
	1.0×10^{11}	1.0×10^{5}	1.0×10^{15}	0.0	1.0×10^{12}	1.0×10^{14}	1.0×10^{10}	1.0×10^{11}	1.0×10^{16}
	1.0×10^{11}	1.0×10^{5}	1.0×10^{18}	0.0	1.0×10^{12}	1.0×10^{14}	1.0×10^{10}	1.0×10^{11}	1.0×10^{16}
	1.0×10^{11}	1.0×10^{11}	1.0×10^{11}	0.0	1.0×10^{12}	1.0×10^{14}	1.0×10^{10}	1.0×10^{11}	1.0×10^{16}
	1.0×10^{11}	1.0×10^{11}	1.0×10^{15}	0.0	1.0×10^{12}	1.0×10^{14}	1.0×10^{10}	1.0×10^{11}	1.0×10^{16}
	1.0×10^{11}	1.0×10^{11}	1.0×10^{18}	0.0	1.0×10^{12}	1.0×10^{14}	1.0×10^{10}	1.0×10^{11}	1.0×10^{16}
	1.0×10^{11}	1.0×10^{19}	1.0×10^{11}	0.0	1.0×10^{12}	1.0×10^{14}	1.0×10^{10}	1.0×10^{11}	1.0×10^{16}
	1.0×10^{11}	1.0×10^{19}	1.0×10^{15}	0.0	1.0×10^{12}	1.0×10^{14}	1.0×10^{10}	1.0×10^{11}	1.0×10^{16}

1.0×10^{11}	1.0×10^{19}	1.0×10^{18}	0.0	1.0×10^{12}	1.0×10^{14}	1.0×10^{10}	1.0×10^{11}	1.0×10^{16}
1.0×10^{11}	0.0	1.0×10^{11}	1.0×10^{9}	1.0×10^{12}	1.0×10^{14}	1.0×10^{10}	1.0×10^{11}	1.0×10^{16}
1.0×10^{11}	0.0	1.0×10^{11}	1.0×10^{13}	1.0×10^{12}	1.0×10^{14}	1.0×10^{10}	1.0×10^{11}	1.0×10^{16}
1.0×10^{11}	0.0	1.0×10^{11}	1.0×10^{17}	1.0×10^{12}	1.0×10^{14}	1.0×10^{10}	1.0×10^{11}	1.0×10^{16}
1.0×10^{11}	0.0	1.0×10^{15}	1.0×10^{9}	1.0×10^{12}	1.0×10^{14}	1.0×10^{10}	1.0×10^{11}	1.0×10^{16}
1.0×10^{11}	0.0	1.0×10^{15}	1.0×10^{13}	1.0×10^{12}	1.0×10^{14}	1.0×10^{10}	1.0×10^{11}	1.0×10^{16}
1.0×10^{11}	0.0	1.0×10^{15}	1.0×10^{17}	1.0×10^{12}	1.0×10^{14}	1.0×10^{10}	1.0×10^{11}	1.0×10^{16}
1.0×10^{11}	0.0	1.0×10^{18}	1.0×10^{9}	1.0×10^{12}	1.0×10^{14}	1.0×10^{10}	1.0×10^{11}	1.0×10^{16}
1.0×10^{11}	0.0	1.0×10^{18}	1.0×10^{13}	1.0×10^{12}	1.0×10^{14}	1.0×10^{10}	1.0×10^{11}	1.0×10^{16}
1.0×10^{11}	0.0	1.0×10^{18}	1.0×10^{17}	1.0×10^{12}	1.0×10^{14}	1.0×10^{10}	1.0×10^{11}	1.0×10^{16}
1.0×10^{11}	1.0×10^{5}	1.0×10^{11}	1.0×10^{9}	1.0×10^{12}	1.0×10^{14}	1.0×10^{10}	1.0×10^{11}	1.0×10^{16}
1.0×10^{11}	1.0×10^{5}	1.0×10^{11}	1.0×10^{13}	1.0×10^{12}	1.0×10^{14}	1.0×10^{10}	1.0×10^{11}	1.0×10^{16}
1.0×10^{11}	1.0×10^{5}	1.0×10^{11}	1.0×10^{17}	1.0×10^{12}	1.0×10^{14}	1.0×10^{10}	1.0×10^{11}	1.0×10^{16}
1.0×10^{11}	1.0×10^{5}	1.0×10^{15}	1.0×10^{9}	1.0×10^{12}	1.0×10^{14}	1.0×10^{10}	1.0×10^{11}	1.0×10^{16}
1.0×10^{11}	1.0×10^{5}	1.0×10^{15}	1.0×10^{13}	1.0×10^{12}	1.0×10^{14}	1.0×10^{10}	1.0×10^{11}	1.0×10^{16}
1.0×10^{11}	1.0×10^{5}	1.0×10^{15}	1.0×10^{17}	1.0×10^{12}	1.0×10^{14}	1.0×10^{10}	1.0×10^{11}	1.0×10^{16}
1.0×10^{11}	1.0×10^{5}	1.0×10^{18}	1.0×10^{9}	1.0×10^{12}	1.0×10^{14}	1.0×10^{10}	1.0×10^{11}	1.0×10^{16}
1.0×10^{11}	1.0×10^{5}	1.0×10^{18}	1.0×10^{13}	1.0×10^{12}	1.0×10^{14}	1.0×10^{10}	1.0×10^{11}	1.0×10^{16}
1.0×10^{11}	1.0×10^{5}	1.0×10^{18}	1.0×10^{17}	1.0×10^{12}	1.0×10^{14}	1.0×10^{10}	1.0×10^{11}	1.0×10^{16}
1.0×10^{11}	1.0×10^{11}	1.0×10^{11}	1.0×10^{9}	1.0×10^{12}	1.0×10^{14}	1.0×10^{10}	1.0×10^{11}	1.0×10^{16}
1.0×10^{11}	1.0×10^{11}	1.0×10^{11}	1.0×10^{13}	1.0×10^{12}	1.0×10^{14}	1.0×10^{10}	1.0×10^{11}	1.0×10^{16}
1.0×10^{11}	1.0×10^{11}	1.0×10^{11}	1.0×10^{17}	1.0×10^{12}	1.0×10^{14}	1.0×10^{10}	1.0×10^{11}	1.0×10^{16}
1.0×10^{11}	1.0×10^{11}	1.0×10^{15}	1.0×10^{9}	1.0×10^{12}	1.0×10^{14}	1.0×10^{10}	1.0×10^{11}	1.0×10^{16}
1.0×10^{11}	1.0×10^{11}	1.0×10^{15}	1.0×10^{13}	1.0×10^{12}	1.0×10^{14}	1.0×10^{10}	1.0×10^{11}	1.0×10^{16}
1.0×10^{11}	1.0×10^{11}	1.0×10^{15}	1.0×10^{17}	1.0×10^{12}	1.0×10^{14}	1.0×10^{10}	1.0×10^{11}	1.0×10^{16}
1.0×10^{11}	1.0×10^{11}	1.0×10^{18}	1.0×10^{9}	1.0×10^{12}	1.0×10^{14}	1.0×10^{10}	1.0×10^{11}	1.0×10^{16}
1.0×10^{11}	1.0×10^{11}	1.0×10^{18}	1.0×10^{13}	1.0×10^{12}	1.0×10^{14}	1.0×10^{10}	1.0×10^{11}	1.0×10^{16}
1.0×10^{11}	1.0×10^{11}	1.0×10^{18}	1.0×10^{17}	1.0×10^{12}	1.0×10^{14}	1.0×10^{10}	1.0×10^{11}	1.0×10^{16}
1.0×10^{11}	1.0×10^{19}	1.0×10^{11}	1.0×10^{9}	1.0×10^{12}	1.0×10^{14}	1.0×10^{10}	1.0×10^{11}	1.0×10^{16}
1.0×10^{11}	1.0×10^{19}	1.0×10^{11}	1.0×10^{13}	1.0×10^{12}	1.0×10^{14}	1.0×10^{10}	1.0×10^{11}	1.0×10^{16}

	1.0×10^{11}	1.0×10^{19}	1.0×10^{11}	1.0×10^{17}	1.0×10^{12}	1.0×10^{14}	1.0×10^{10}	1.0×10^{11}	1.0×10^{16}
	1.0×10^{11}	1.0×10^{19}	1.0×10^{15}	1.0×10^{9}	1.0×10^{12}	1.0×10^{14}	1.0×10^{10}	1.0×10^{11}	1.0×10^{16}
	1.0×10^{11}	1.0×10^{19}	1.0×10^{15}	1.0×10^{13}	1.0×10^{12}	1.0×10^{14}	1.0×10^{10}	1.0×10^{11}	1.0×10^{16}
	1.0×10^{11}	1.0×10^{19}	1.0×10^{15}	1.0×10^{17}	1.0×10^{12}	1.0×10^{14}	1.0×10^{10}	1.0×10^{11}	1.0×10^{16}
	1.0×10^{11}	1.0×10^{19}	1.0×10^{18}	1.0×10^{9}	1.0×10^{12}	1.0×10^{14}	1.0×10^{10}	1.0×10^{11}	1.0×10^{16}
	1.0×10^{11}	1.0×10^{19}	1.0×10^{18}	1.0×10^{13}	1.0×10^{12}	1.0×10^{14}	1.0×10^{10}	1.0×10^{11}	1.0×10^{16}
	1.0×10^{11}	1.0×10^{19}	1.0×10^{18}	1.0×10^{17}	1.0×10^{12}	1.0×10^{14}	1.0×10^{10}	1.0×10^{11}	1.0×10^{16}

Table S6. Description of global model experiments.

Scheme	Description
Case0	Run with three initial oxidation pathways
Case1	The same as Case0 without OH-initial oxidation pathway
Case2	The same as Case0 without O_3-initial oxidation pathway
Case3	The same as Case0 without NO_3-initial oxidation pathway
Case4	The same as Case0 without O_3 and NO_3-initial oxidation pathways
Case5	The same as Case0 without OH and NO_3-initial oxidation pathways
Case6	The same as Case0 without OH and O_3-initial oxidation pathways

Table S7. Estimated reaction rates under two initial oxidation pathway experiments

Test description				Reaction rates ($cm^{-3}\cdot s^{-1}$)		
Scheme	Variables (cm^{-3})			R_{OH}	R_{O3}	R_{NO3}
	OH	O_3	NO_3			
$OH + O_3$	1.0×10^{5}	0.0	/	2.4×10^{10}	4.8×10^{4}	/
	1.0×10^{5}	1.0×10^{11}	/	2.3×10^{10}	8.6×10^{7}	/
	1.0×10^{5}	1.0×10^{15}	/	1.4×10^{10}	7.9×10^{10}	/
	1.0×10^{5}	1.0×10^{20}	/	3.2×10^{7}	1.0×10^{11}	/
	1.0×10^{19}	0.0	/	4.4×10^{10}	1.4×10^{5}	/
	1.0×10^{19}	1.0×10^{11}	/	4.4×10^{10}	6.3×10^{7}	/
	1.0×10^{19}	1.0×10^{15}	/	1.9×10^{10}	7.5×10^{10}	/
	1.0×10^{19}	1.0×10^{20}	/	4.1×10^{7}	1.0×10^{11}	/
	1.0×10^{35}	0.0	/	1.0×10^{11}	3.3×10^{6}	/
	1.0×10^{35}	1.0×10^{11}	/	1.0×10^{11}	3.3×10^{6}	/
	1.0×10^{35}	1.0×10^{15}	/	1.0×10^{11}	3.3×10^{6}	/
	1.0×10^{35}	1.0×10^{20}	/	1.0×10^{11}	7.6×10^{6}	/
$OH + NO_3$	1.0×10^{5}	/	0.0	5.4×10^{10}	/	2.4×10^{5}
	1.0×10^{5}	/	1.0×10^{9}	5.4×10^{10}	/	2.5×10^{7}
	1.0×10^{5}	/	1.0×10^{13}	4.9×10^{8}	/	9.9×10^{10}
	1.0×10^{5}	/	1.0×10^{18}	2.0×10^{4}	/	1.0×10^{11}
	1.0×10^{19}	/	0.0	7.4×10^{10}	/	1.1×10^{6}
	1.0×10^{19}	/	1.0×10^{9}	7.4×10^{10}	/	1.7×10^{7}
	1.0×10^{19}	/	1.0×10^{13}	9.7×10^{8}	/	9.9×10^{10}
	1.0×10^{19}	/	1.0×10^{18}	3.5×10^{4}	/	1.0×10^{11}
	1.0×10^{35}	/	0.0	1.0×10^{11}	/	1.5×10^{6}
	1.0×10^{35}	/	1.0×10^{9}	1.0×10^{11}	/	1.5×10^{6}
	1.0×10^{35}	/	1.0×10^{13}	1.0×10^{11}	/	1.5×10^{6}
	1.0×10^{35}	/	1.0×10^{18}	9.8×10^{10}	/	2.1×10^{9}
$O_3 + OH$	0.0	1.0×10^{11}	/	2.3×10^{10}	8.6×10^{7}	/
	1.0×10^{5}	1.0×10^{11}	/	2.3×10^{10}	8.6×10^{7}	/

	1.0×10^{19}	1.0×10^{11}	/	4.4×10^{10}	6.3×10^{7}	/
	1.0×10^{35}	1.0×10^{11}	/	1.0×10^{11}	3.3×10^{6}	/
	0.0	1.0×10^{15}	/	1.4×10^{10}	7.9×10^{10}	/
	1.0×10^{5}	1.0×10^{15}	/	1.4×10^{10}	7.9×10^{10}	/
	1.0×10^{19}	1.0×10^{15}	/	1.9×10^{10}	7.5×10^{10}	/
	1.0×10^{35}	1.0×10^{15}	/	1.0×10^{11}	3.3×10^{6}	/
	0.0	1.0×10^{20}	/	3.2×10^{7}	1.0×10^{11}	/
	1.0×10^{5}	1.0×10^{20}	/	3.2×10^{7}	1.0×10^{11}	/
	1.0×10^{19}	1.0×10^{20}	/	4.1×10^{7}	1.0×10^{11}	/
	1.0×10^{35}	1.0×10^{20}	/	1.0×10^{11}	7.6×10^{6}	/
$O_3 + NO_3$	/	1.0×10^{11}	0.0	/	7.8×10^{7}	1.0×10^{7}
	/	1.0×10^{11}	1.0×10^{9}	/	7.7×10^{7}	8.8×10^{7}
	/	1.0×10^{11}	1.0×10^{13}	/	1.1×10^{5}	1.0×10^{11}
	/	1.0×10^{11}	1.0×10^{18}	/	3.4×10^{2}	1.0×10^{11}
	/	1.0×10^{15}	0.0	/	3.3×10^{10}	6.5×10^{10}
	/	1.0×10^{15}	1.0×10^{9}	/	3.3×10^{10}	6.5×10^{10}
	/	1.0×10^{15}	1.0×10^{13}	/	1.0×10^{9}	9.9×10^{10}
	/	1.0×10^{15}	1.0×10^{18}	/	1.3×10^{6}	1.0×10^{11}
	/	1.0×10^{20}	0.0	/	8.4×10^{10}	1.6×10^{10}
	/	1.0×10^{20}	1.0×10^{9}	/	8.4×10^{10}	1.6×10^{10}
	/	1.0×10^{20}	1.0×10^{13}	/	7.0×10^{10}	3.0×10^{10}
	/	1.0×10^{20}	1.0×10^{18}	/	1.2×10^{9}	9.9×10^{10}
$NO_3 + OH$	0.0	/	1.0×10^{9}	5.4×10^{10}	/	2.5×10^{7}
	1.0×10^{5}	/	1.0×10^{9}	5.4×10^{10}	/	2.5×10^{7}
	1.0×10^{19}	/	1.0×10^{9}	7.4×10^{10}	/	1.7×10^{7}
	1.0×10^{35}	/	1.0×10^{9}	1.0×10^{11}	/	1.5×10^{6}
	0.0	/	1.0×10^{13}	4.9×10^{8}	/	9.9×10^{10}
	1.0×10^{5}	/	1.0×10^{13}	4.9×10^{8}	/	9.9×10^{10}
	1.0×10^{19}	/	1.0×10^{13}	9.7×10^{8}	/	9.9×10^{10}
	1.0×10^{35}	/	1.0×10^{13}	1.0×10^{11}	/	1.5×10^{6}

	0.0	/	1.0×10^{18}	2.0×10^{4}	/	1.0×10^{11}
	1.0×10^{5}	/	1.0×10^{18}	2.0×10^{4}	/	1.0×10^{11}
	1.0×10^{19}	/	1.0×10^{18}	3.5×10^{4}	/	1.0×10^{11}
	1.0×10^{35}	/	1.0×10^{18}	9.8×10^{10}	/	2.0×10^{9}
$NO_3 + O_3$	/	0.0	1.0×10^{9}	/	4.2×10^{3}	8.0×10^{7}
	/	1.0×10^{11}	1.0×10^{9}	/	7.7×10^{7}	8.8×10^{7}
	/	1.0×10^{15}	1.0×10^{9}	/	3.3×10^{10}	6.5×10^{10}
	/	1.0×10^{20}	1.0×10^{9}	/	8.4×10^{10}	1.6×10^{10}
	/	0.0	1.0×10^{13}		1.1×10^{3}	1.0×10^{11}
	/	1.0×10^{11}	1.0×10^{13}	/	1.1×10^{5}	1.0×10^{11}
	/	1.0×10^{15}	1.0×10^{13}	/	1.0×10^{9}	9.9×10^{10}
	/	1.0×10^{20}	1.0×10^{13}	/	7.0×10^{10}	3.0×10^{10}
	/	0.0	1.0×10^{18}	/	1.9×10^{-1}	1.0×10^{11}
	/	1.0×10^{11}	1.0×10^{18}	/	3.4×10^{2}	1.0×10^{11}
	/	1.0×10^{15}	1.0×10^{18}	/	1.3×10^{6}	1.0×10^{11}
	/	1.0×10^{20}	1.0×10^{18}	/	1.2×10^{9}	9.9×10^{10}

Table S8. Estimated reaction rates under three initial oxidation pathway experiments.

Test description				Reaction rates (·cm^{-3}·s^{-1})		
Scheme	Variables (molecucm^{-3})			R_{OH}	R_{O3}	R_{NO3}
	OH	O_3	NO_3			
The influence of OH-initiated oxidation pathway	0.0	1.0×10^{11}	1.0×10^{9}	5.2×10^{10}	3.5×10^{7}	3.7×10^{7}
	1.0×10^{5}	1.0×10^{11}	1.0×10^{9}	5.2×10^{10}	3.5×10^{7}	3.7×10^{7}
	1.0×10^{11}	1.0×10^{11}	1.0×10^{9}	7.0×10^{10}	2.5×10^{7}	3.6×10^{7}
	1.0×10^{19}	1.0×10^{11}	1.0×10^{9}	1.0×10^{11}	3.3×10^{6}	1.4×10^{6}
	0.0	1.0×10^{15}	1.0×10^{9}	2.6×10^{9}	3.1×10^{10}	6.3×10^{10}
	1.0×10^{5}	1.0×10^{15}	1.0×10^{9}	2.6×10^{9}	3.1×10^{10}	6.3×10^{10}
	1.0×10^{11}	1.0×10^{15}	1.0×10^{9}	5.0×10^{9}	3.2×10^{10}	6.1×10^{10}
	1.0×10^{19}	1.0×10^{15}	1.0×10^{9}	1.0×10^{11}	3.3×10^{6}	2.6×10^{5}
	0.0	1.0×10^{18}	1.0×10^{9}	2.5×10^{7}	8.5×10^{10}	1.6×10^{10}
	1.0×10^{5}	1.0×10^{18}	1.0×10^{9}	2.5×10^{7}	8.5×10^{10}	1.6×10^{10}
	1.0×10^{11}	1.0×10^{18}	1.0×10^{9}	3.1×10^{7}	8.0×10^{10}	2.0×10^{10}
	1.0×10^{19}	1.0×10^{18}	1.0×10^{9}	1.0×10^{11}	7.6×10^{6}	1.5×10^{6}
	0.0	1.0×10^{11}	1.0×10^{13}	4.0×10^{8}	1.1×10^{5}	1.0×10^{11}
	1.0×10^{5}	1.0×10^{11}	1.0×10^{13}	4.0×10^{8}	1.1×10^{5}	1.0×10^{11}
	1.0×10^{11}	1.0×10^{11}	1.0×10^{13}	7.2×10^{8}	1.4×10^{5}	9.9×10^{10}
	1.0×10^{19}	1.0×10^{11}	1.0×10^{13}	1.0×10^{11}	3.3×10^{6}	1.4×10^{6}
	0.0	1.0×10^{15}	1.0×10^{13}	2.9×10^{8}	9.9×10^{8}	9.9×10^{10}
	1.0×10^{5}	1.0×10^{15}	1.0×10^{13}	2.9×10^{8}	9.9×10^{8}	9.9×10^{10}
	1.0×10^{11}	1.0×10^{15}	1.0×10^{13}	5.3×10^{8}	1.4×10^{9}	9.8×10^{10}
	1.0×10^{19}	1.0×10^{15}	1.0×10^{13}	1.0×10^{11}	3.3×10^{6}	3.0×10^{5}
	0.0	1.0×10^{18}	1.0×10^{13}	2.0×10^{7}	7.0×10^{10}	3.0×10^{10}
	1.0×10^{5}	1.0×10^{18}	1.0×10^{13}	2.0×10^{7}	7.0×10^{10}	3.0×10^{10}
	1.0×10^{11}	1.0×10^{18}	1.0×10^{13}	2.7×10^{7}	7.0×10^{10}	3.0×10^{10}
	1.0×10^{19}	1.0×10^{18}	1.0×10^{13}	1.0×10^{11}	7.6×10^{6}	1.6×10^{6}
	0.0	1.0×10^{11}	1.0×10^{17}	2.0×10^{4}	3.4×10^{2}	1.0×10^{11}
	1.0×10^{5}	1.0×10^{11}	1.0×10^{17}	2.0×10^{4}	3.4×10^{2}	1.0×10^{11}

	1.0×10^{11}	1.0×10^{11}	1.0×10^{17}	3.5×10^{4}	3.1×10^{2}	1.0×10^{11}
	1.0×10^{19}	1.0×10^{11}	1.0×10^{17}	9.8×10^{10}	3.2×10^{6}	2.0×10^{9}
	0.0	1.0×10^{15}	1.0×10^{17}	7.7×10^{3}	1.3×10^{6}	1.0×10^{11}
	1.0×10^{5}	1.0×10^{15}	1.0×10^{17}	7.7×10^{3}	1.3×10^{6}	1.0×10^{11}
	1.0×10^{11}	1.0×10^{15}	1.0×10^{17}	1.5×10^{4}	1.3×10^{6}	1.0×10^{11}
	1.0×10^{19}	1.0×10^{15}	1.0×10^{17}	9.8×10^{10}	3.2×10^{6}	2.0×10^{9}
	0.0	1.0×10^{18}	1.0×10^{17}	6.6×10^{3}	1.2×10^{9}	9.9×10^{10}
	1.0×10^{5}	1.0×10^{18}	1.0×10^{17}	6.6×10^{3}	1.2×10^{9}	9.9×10^{10}
	1.0×10^{11}	1.0×10^{18}	1.0×10^{17}	1.3×10^{4}	1.2×10^{9}	9.9×10^{10}
	1.0×10^{19}	1.0×10^{18}	1.0×10^{17}	9.7×10^{10}	1.4×10^{7}	2.9×10^{9}
The influence of O_3-initiated oxidation pathway	1.0×10^{5}	0.0	1.0×10^{9}	5.2×10^{10}	7.6×10^{4}	3.3×10^{7}
	1.0×10^{5}	1.0×10^{11}	1.0×10^{9}	5.2×10^{10}	3.5×10^{7}	3.7×10^{7}
	1.0×10^{5}	1.0×10^{15}	1.0×10^{9}	2.6×10^{9}	3.1×10^{10}	6.3×10^{10}
	1.0×10^{5}	1.0×10^{20}	1.0×10^{9}	2.5×10^{7}	8.5×10^{10}	1.5×10^{10}
	1.0×10^{11}	0.0	1.0×10^{9}	7.0×10^{10}	1.6×10^{5}	3.3×10^{7}
	1.0×10^{11}	1.0×10^{11}	1.0×10^{9}	7.0×10^{10}	2.5×10^{7}	3.6×10^{7}
	1.0×10^{11}	1.0×10^{15}	1.0×10^{9}	5.0×10^{9}	3.2×10^{10}	6.1×10^{10}
	1.0×10^{11}	1.0×10^{20}	1.0×10^{9}	3.1×10^{7}	8.0×10^{10}	2.0×10^{10}
	1.0×10^{19}	0.0	1.0×10^{9}	1.0×10^{11}	3.3×10^{6}	1.5×10^{6}
	1.0×10^{19}	1.0×10^{11}	1.0×10^{9}	1.0×10^{11}	3.3×10^{6}	1.4×10^{6}
	1.0×10^{19}	1.0×10^{15}	1.0×10^{9}	1.0×10^{11}	3.3×10^{6}	2.6×10^{5}
	1.0×10^{19}	1.0×10^{20}	1.0×10^{9}	1.0×10^{11}	7.6×10^{6}	1.5×10^{6}
	1.0×10^{5}	0.0	1.0×10^{13}	3.9×10^{8}	1.0×10^{3}	1.0×10^{11}
	1.0×10^{5}	1.0×10^{11}	1.0×10^{13}	4.0×10^{8}	1.1×10^{5}	1.0×10^{11}
	1.0×10^{5}	1.0×10^{15}	1.0×10^{13}	2.9×10^{8}	9.9×10^{8}	9.9×10^{10}
	1.0×10^{5}	1.0×10^{20}	1.0×10^{13}	2.0×10^{7}	7.0×10^{10}	3.0×10^{10}
	1.0×10^{11}	0.0	1.0×10^{13}	7.1×10^{8}	1.7×10^{3}	9.9×10^{10}
	1.0×10^{11}	1.0×10^{11}	1.0×10^{13}	7.2×10^{8}	1.4×10^{5}	9.9×10^{10}
	1.0×10^{11}	1.0×10^{15}	1.0×10^{13}	5.3×10^{8}	1.4×10^{9}	9.8×10^{10}
	1.0×10^{11}	1.0×10^{20}	1.0×10^{13}	2.7×10^{7}	7.0×10^{10}	3.0×10^{10}

	1.0×10^{19}	0.0	1.0×10^{13}	1.0×10^{11}	3.3×10^{6}	1.5×10^{6}
	1.0×10^{19}	1.0×10^{11}	1.0×10^{13}	1.0×10^{11}	3.3×10^{6}	1.4×10^{6}
	1.0×10^{19}	1.0×10^{15}	1.0×10^{13}	1.0×10^{11}	3.3×10^{6}	3.0×10^{5}
	1.0×10^{19}	1.0×10^{20}	1.0×10^{13}	1.0×10^{11}	7.6×10^{6}	1.6×10^{6}
	1.0×10^{5}	0.0	1.0×10^{18}	2.0×10^{4}	1.8×10^{-1}	1.0×10^{11}
	1.0×10^{5}	1.0×10^{11}	1.0×10^{18}	2.0×10^{4}	3.4×10^{2}	1.0×10^{11}
	1.0×10^{5}	1.0×10^{15}	1.0×10^{18}	7.7×10^{3}	1.3×10^{6}	1.0×10^{11}
	1.0×10^{5}	1.0×10^{20}	1.0×10^{18}	6.6×10^{3}	1.2×10^{9}	9.9×10^{10}
	1.0×10^{11}	0.0	1.0×10^{18}	3.5×10^{4}	2.9×10^{-1}	1.0×10^{11}
	1.0×10^{11}	1.0×10^{11}	1.0×10^{18}	3.5×10^{4}	3.1×10^{2}	1.0×10^{11}
	1.0×10^{11}	1.0×10^{15}	1.0×10^{18}	1.5×10^{4}	1.3×10^{6}	1.0×10^{11}
	1.0×10^{11}	1.0×10^{20}	1.0×10^{18}	1.3×10^{4}	1.2×10^{9}	9.9×10^{10}
	1.0×10^{19}	0.0	1.0×10^{18}	9.8×10^{10}	3.2×10^{6}	2.0×10^{9}
	1.0×10^{19}	1.0×10^{11}	1.0×10^{18}	9.8×10^{10}	3.2×10^{6}	2.0×10^{9}
	1.0×10^{19}	1.0×10^{15}	1.0×10^{18}	9.8×10^{10}	3.2×10^{6}	2.0×10^{9}
	1.0×10^{19}	1.0×10^{20}	1.0×10^{18}	9.7×10^{10}	1.4×10^{7}	2.9×10^{9}
The influence of NO_3-initiated oxidation pathway	1.0×10^{5}	1.0×10^{11}	0.0	5.2×10^{10}	3.5×10^{7}	2.0×10^{6}
	1.0×10^{5}	1.0×10^{11}	1.0×10^{9}	5.2×10^{10}	3.5×10^{7}	3.7×10^{7}
	1.0×10^{5}	1.0×10^{11}	1.0×10^{13}	4.0×10^{8}	1.1×10^{5}	1.0×10^{11}
	1.0×10^{5}	1.0×10^{11}	1.0×10^{18}	2.0×10^{4}	3.4×10^{2}	1.0×10^{11}
	1.0×10^{19}	1.0×10^{11}	0.0	7.0×10^{10}	2.5×10^{7}	5.6×10^{6}
	1.0×10^{19}	1.0×10^{11}	1.0×10^{9}	7.0×10^{10}	2.5×10^{7}	3.6×10^{7}
	1.0×10^{19}	1.0×10^{11}	1.0×10^{13}	7.2×10^{8}	1.4×10^{5}	9.9×10^{10}
	1.0×10^{19}	1.0×10^{11}	1.0×10^{18}	3.5×10^{4}	3.1×10^{2}	1.0×10^{11}
	1.0×10^{35}	1.0×10^{11}	0.0	1.0×10^{11}	3.3×10^{6}	1.4×10^{6}
	1.0×10^{35}	1.0×10^{11}	1.0×10^{9}	1.0×10^{11}	3.3×10^{6}	1.4×10^{6}
	1.0×10^{35}	1.0×10^{11}	1.0×10^{13}	1.0×10^{11}	3.3×10^{6}	1.4×10^{6}
	1.0×10^{35}	1.0×10^{11}	1.0×10^{18}	9.8×10^{10}	3.2×10^{6}	2.0×10^{9}
	1.0×10^{5}	1.0×10^{15}	0.0	2.6×10^{9}	3.1×10^{10}	6.3×10^{10}
	1.0×10^{5}	1.0×10^{15}	1.0×10^{9}	2.6×10^{9}	3.1×10^{10}	6.3×10^{10}

1.0×10^{5}	1.0×10^{15}	1.0×10^{13}	2.9×10^{8}	9.9×10^{8}	9.9×10^{10}
1.0×10^{5}	1.0×10^{15}	1.0×10^{18}	7.7×10^{3}	1.3×10^{6}	1.0×10^{11}
1.0×10^{19}	1.0×10^{15}	0.0	5.0×10^{9}	3.2×10^{10}	6.0×10^{10}
1.0×10^{19}	1.0×10^{15}	1.0×10^{9}	5.0×10^{9}	3.2×10^{10}	6.1×10^{10}
1.0×10^{19}	1.0×10^{15}	1.0×10^{13}	5.3×10^{8}	1.4×10^{9}	9.8×10^{10}
1.0×10^{19}	1.0×10^{15}	1.0×10^{18}	1.5×10^{4}	1.3×10^{6}	1.0×10^{11}
1.0×10^{35}	1.0×10^{15}	0.0	1.0×10^{11}	3.3×10^{6}	2.6×10^{5}
1.0×10^{35}	1.0×10^{15}	1.0×10^{9}	1.0×10^{11}	3.3×10^{6}	2.6×10^{5}
1.0×10^{35}	1.0×10^{15}	1.0×10^{13}	1.0×10^{11}	3.3×10^{6}	3.0×10^{5}
1.0×10^{35}	1.0×10^{15}	1.0×10^{18}	9.8×10^{10}	3.2×10^{6}	2.0×10^{9}
1.0×10^{5}	1.0×10^{20}	0.0	2.5×10^{7}	8.5×10^{10}	1.5×10^{10}
1.0×10^{5}	1.0×10^{20}	1.0×10^{9}	2.5×10^{7}	8.5×10^{10}	1.5×10^{10}
1.0×10^{5}	1.0×10^{20}	1.0×10^{13}	2.0×10^{7}	7.0×10^{10}	3.0×10^{10}
1.0×10^{5}	1.0×10^{20}	1.0×10^{18}	6.6×10^{3}	1.2×10^{9}	9.9×10^{10}
1.0×10^{19}	1.0×10^{20}	0.0	3.1×10^{7}	8.0×10^{10}	2.0×10^{10}
1.0×10^{19}	1.0×10^{20}	1.0×10^{9}	3.1×10^{7}	8.0×10^{10}	2.0×10^{10}
1.0×10^{19}	1.0×10^{20}	1.0×10^{13}	2.7×10^{7}	7.0×10^{10}	3.0×10^{10}
1.0×10^{19}	1.0×10^{20}	1.0×10^{18}	1.3×10^{4}	1.2×10^{9}	9.9×10^{10}
1.0×10^{35}	1.0×10^{20}	0.0	1.0×10^{11}	7.6×10^{6}	1.5×10^{6}
1.0×10^{35}	1.0×10^{20}	1.0×10^{9}	1.0×10^{11}	7.6×10^{6}	1.5×10^{6}
1.0×10^{35}	1.0×10^{20}	1.0×10^{13}	1.0×10^{11}	7.6×10^{6}	1.6×10^{6}
1.0×10^{35}	1.0×10^{20}	1.0×10^{18}	9.7×10^{10}	1.5×10^{7}	2.9×10^{9}

Table S9. Published measurements of atmospheric particulate ON concentrations at surface sites.

Area	Site	Observation period	ON (ug·m^{-3})	Reference
Urban	Bakersfield, California, USA	15 May - 24 Jun 2010	0.51	(Rollins et al., 2012)
Urban	Bakersfield, California, USA	15 May - 24 Jun 2010	0.46	(Rollins et al., 2013)
Urban	Atlanta, Georgia, USA	May 2012 - Feb 2013	0.7	(Xu et al., 2015)
Urban	San Antonio, Texas, USA	May 2 to 26, 2017	0.17	(Guo et al., 2024)
Urban	Ji'nan, China	Apr 2016	0.26	(Li et al., 2018)
Urban	Shenzhen, China	2005 - 2006	0.51	(Yu et al., 2019)
Urban	Shenzhen, China	Spring	0.5	(Yu et al., 2019)
Urban	Shenzhen, China	Summer	1.4	(Yu et al., 2019)
Urban	Shenzhen, China	Autumn	0.87	(Yu et al., 2019)
Urban	Beijing, China	20 May - 23 Jun 2018, 20 Nov - 25 Dec 2018	3	(Xu et al., 2021)
Urban	Beijing, China	20 May - 23 Jun 2018, 20 Nov - 25 Dec 2018	0.9	(Xu et al., 2021)
Urban	Xi'an, China	29 Oct to 19 Nov, 2020	3.57	(Lin et al., 2021)
Urban	Nanjing, China	Apr 2020	1.22	(Ge et al., 2022)
Urban	Nanjing, China	Jul 2019	0.62	(Ge et al., 2022)
Urban	Nanjing, China	Oct 2019	1.24	(Ge et al., 2022)
Urban	Nanjing, China	Dec	2.91	(Ge et al., 2022)
Urban	Barcelona, Spain	1 - 26 Mar 2009	1.57	(Mohr et al., 2012)
Urban	Helsinki, Finland	9 Jan - 13 Mar 2009	0.46	(Carbone et al., 2014)
Rural	Centreville, Alabama, USA	1 Jun - 15 Jul 2013	0.23	(Xu et al., 2015)
Rural	Yorkville, Georgia, USA	26 Jun - 20 Jul 2013	0.6	(Xu et al., 2015)
Rural	Changping, China	15 May - 23 Jun 2016	0.01	(Wang et al., 2018)
Rural	Xianghe, China	25 Dec 2018 - 13 Jan 2019	2.29	(Huang et al., 2021)
Rural	Xianghe, China	9 Jun to 9 Jul 2013	1.86	(Zhu et al., 2021)
Rural	Xianghe, China	9 Jun to 9 Jul 2013	1.71	(Zhu et al., 2021)
Rural	Gucheng, China	10 Dec 2019 - 13 Jan 2020	6.14	(Xu et al., 2021)
Rural	Wanqingsha, China	1 - 30 Sep, 1 - 26 Nov 2010	0.07	(He et al., 2014)
Rural	Cabauw, Netherlands	May 2008	1.71	(Mensah et al., 2012)

Rural	Cabauw, Netherlands	Mar 2009	1.23	(Mensah et al., 2012)
Rural	Jungfraujoch, Switzerland	30 Apr - 29 May 2008	0.1	(Lanz et al., 2010)
Rural	Melpitz, Germany	23 May - 9 Jun 2008	1.01	(Poulain et al., 2011)
Rural	Melpitz, Germany	16 Sep - 3 Nov 2008	2.39	(Poulain et al., 2011)
Rural	Melpitz, Germany	24 Feb - 27 Mar 2009	2.23	(Poulain et al., 2011)
Rural	Payerne, Swiss	Oct 2008	0.64	(Kiendler-Scharr et al., 2016)
Rural	Payerne, Swiss	Mar 2009	2.29	(Kiendler-Scharr et al., 2016)
Rural	Puijo, Finland	Oct 2008	0.23	(Kiendler-Scharr et al., 2016)
Rural	San Pietro Capofiume, Italy	30 Mar - 20 Apr 2008	3.87	(Saarikoski et al., 2012)
Rural	Po Valley, Italy	Oct 2008	2.41	(Kiendler-Scharr et al., 2016)
Rural	Po Valley, Italy	Mar 2009	3.16	(Kiendler-Scharr et al., 2016)
Rural	Harwell HW/GB36	Oct 2008	2.9	(Kiendler-Scharr et al., 2016)
Rural	Hyytiälä, Finland	Oct 2008	0.29	(Kiendler-Scharr et al., 2016)
Rural	Hyytiälä, Finland	Mar 2009	0.29	(Kiendler-Scharr et al., 2016)
Rural	Kpuszta KPO/HU02	Oct 2008	1.39	(Kiendler-Scharr et al., 2016)
Rural	Montseny, Spain	25 Feb - 26 Mar 2009	3.16	(Minguillón et al., 2011)
Rural	Puy de Dome, France	Oct 2008	0.74	(Freney et al., 2011)
Rural	Puy de Dome, France	Mar 2009	0.51	(Freney et al., 2011)
Forest	Woodland Park, Colorado, USA	Jul - Aug 2011	0.2	(Fry et al., 2014)
Forest	Tuscaloosa, Alabama, USA	1 Jun - 15 Jul 2013	0.8	(Ayres et al., 2015)
Forest	Hyytiälä, Finland	Apr 8 and May 4, 2016	0.32	(Graeffe et al., 2023)
Coastal	Connemara, Ireland	May 2008	0.16	(Dall'osto et al., 2010)
Coastal	Finokalia, Crete, Greece	4 May-8 Jun 2008	0.2	(Pikridas et al., 2010)
Coastal	Finokalia, Crete, Greece	25 Feb - 26 Mar 2009	0.1	(Hildebrandt et al., 2011)

Table S10. The NMB between observation and simulation and in different schemes.

Scheme	Observation ($ng \cdot m^{-3}$)	Simulation ($ng \cdot m^{-3}$)	NMB[a]	Description
1	1296.2	90.2	-93.0%	Exclusion of the limonene-derived ON formation
2	1296.2	192.2	-85.2%	Incorporation of the limonene-derived ON formation

[a]NMB = normalized mean bias

References

Ayres, B. R., Allen, H. M., Draper, D. C., Brown, S. S., Wild, R. J., Jimenez, J. L., Day, D. A., Campuzano-Jost, P., Hu, W., de Gouw, J., Koss, A., Cohen, R. C., Duffey, K. C., Romer, P., Baumann, K., Edgerton, E., Takahama, S., Thornton, J. A., Lee, B. H., Lopez-Hilfiker, F. D., Mohr, C., Wennberg, P. O., Nguyen, T. B., Teng, A., Goldstein, A. H., Olson, K., and Fry, J. L.: Organic nitrate aerosol formation via NO_3 + biogenic volatile organic compounds in the southeastern United States, Atmos. Chem. Phys., 15, 13377-13392, https://doi.org/10.5194/acp-15-13377-2015, 2015.

Carbone, S., Aurela, M., Saarnio, K., Saarikoski, S., Timonen, H., Frey, A., Sueper, D., Ulbrich, I. M., Jimenez, J. L., Kulmala, M., Worsnop, D. R., and Hillamo, R. E.: Wintertime Aerosol Chemistry in Sub-Arctic Urban Air, Aerosol Sci. Technol., 48, 313-323, https://doi.org/10.1080/02786826.2013.875115, 2014.

Dall'Osto, M., Ceburnis, D., Martucci, G., Bialek, J., Dupuy, R., Jennings, S. G., Berresheim, H., Wenger, J., Healy, R., Facchini, M. C., Rinaldi, M., Giulianelli, L., Finessi, E., Worsnop, D., Ehn, M., Mikkilä, J., Kulmala, M., and O'Dowd, C. D.: Aerosol properties associated with air masses arriving into the North East Atlantic during the 2008 Mace Head EUCAARI intensive observing period: an overview, Atmos. Chem. Phys., 10, 8413-8435, https://doi.org/10.5194/acp-10-8413-2010, 2010.

Freney, E. J., Sellegri, K., Canonaco, F., Boulon, J., Hervo, M., Weigel, R., Pichon, J. M., Colomb, A., Prévôt, A. S. H., and Laj, P.: Seasonal variations in aerosol particle composition at the puy-de-Dôme research station in France, Atmos. Chem. Phys., 11, 13047-13059, https://doi.org/10.5194/acp-11-13047-2011, 2011.

Fry, J. L., Draper, D. C., Barsanti, K. C., Smith, J. N., Ortega, J., Winkler, P. M., Lawler, M. J., Brown, S. S., Edwards, P. M., Cohen, R. C., and Lee, L.: Secondary Organic Aerosol Formation and Organic Nitrate Yield from NO_3 Oxidation of Biogenic Hydrocarbons, Environ. Sci. Technol., 48, 11944-11953, https://doi.org/10.1021/es502204x, 2014.

Ge, D., Nie, W., Sun, P., Liu, Y., Wang, T., Wang, J., Wang, J., Wang, L., Zhu, C., Wang, R., Liu, T., Chi, X., and Ding, A.: Characterization of particulate organic nitrates in the Yangtze River Delta, East China, using the time-of-flight aerosol chemical speciation monitor, Atmos. Environ., 272, https://doi.org/10.1016/j.atmosenv.2021.118927, 2022.

Graeffe, F., Heikkinen, L., Garmash, O., Aijala, M., Allan, J., Feron, A., Cirtog, M., Petit, J. E., Bonnaire, N., Lambe, A., Favez, O., Albinet, A., Williams, L. R., and Ehn, M.: Detecting and Characterizing Particulate Organic Nitrates with an Aerodyne Long-ToF Aerosol Mass Spectrometer, ACS Earth Space Chem., 7, 230-242, https://doi.org/10.1021/acsearthspacechem.2c00314, 2023.

Guo, F., Bui, A. A. T., Schulze, B. C., Dai, Q., Yoon, S., Shrestha, S., Wallace, H. W., Sanchez, N. P., Alvarez, S., Erickson, M. H., Sheesley, R. J., Usenko, S., Flynn, J., and Griffin, R. J.: Airmass History, Night-Time Particulate Organonitrates, and Meteorology Impact Urban SOA Formation Rate, Atmos. Environ., 322, https://doi.org/10.1016/j.atmosenv.2024.120362, 2024.

He, Q. F., Ding, X., Wang, X. M., Yu, J. Z., Fu, X. X., Liu, T. Y., Zhang, Z., Xue, J., Chen, D. H., Zhong, L. J., and Donahue, N. M.: Organosulfates from pinene and isoprene over the Pearl River Delta, South China: seasonal variation and implication in formation mechanisms, Environ. Sci. Technol., 48, 9236-9245, https://doi.org/10.1021/es501299v, 2014.

Hildebrandt, L., Kostenidou, E., Lanz, V. A., Prevot, A. S. H., Baltensperger, U., Mihalopoulos, N., Laaksonen, A., Donahue, N. M., and Pandis, S. N.: Sources and atmospheric processing of organic aerosol in the Mediterranean: insights from aerosol mass spectrometer factor analysis, Atmos. Chem. Phys., 11, 12499-12515, https://doi.org/10.5194/acp-11-12499-2011, 2011.

Huang, W., Yang, Y., Wang, Y., Gao, W., Li, H., Zhang, Y., Li, J., Zhao, S., Yan, Y., Ji, D., Tang, G., Liu, Z., Wang, L., Zhang, R., and Wang, Y.: Exploring the inorganic and organic nitrate aerosol formation regimes at a suburban site on the North China Plain, Sci. Total Environ., 768, 144538, https://doi.org/10.1016/j.scitotenv.2020.144538, 2021.

Kiendler-Scharr, A., Mensah, A. A., Friese, E., Topping, D., Nemitz, E., Prevot, A. S. H., Äijälä, M., Allan, J., Canonaco, F., Canagaratna, M., Carbone, S., Crippa, M., Dall Osto, M., Day, D. A., De Carlo, P., Di Marco, C. F., Elbern, H., Eriksson, A., Freney, E., Hao, L., Herrmann, H., Hildebrandt, L., Hillamo, R., Jimenez, J. L., Laaksonen, A., McFiggans, G., Mohr, C., O'Dowd, C., Otjes, R., Ovadnevaite, J., Pandis, S. N., Poulain, L., Schlag, P., Sellegri, K., Swietlicki, E., Tiitta, P., Vermeulen, A., Wahner, A., Worsnop, D., and Wu, H. C.: Ubiquity of Organic Nitrates from Nighttime Chemistry in the European Submicron Aerosol, Geophys. Res. Lett., 43, 7735-7744, https://doi.org/10.1002/2016gl069239, 2016.

Lanz, V. A., Prévôt, A. S. H., Alfarra, M. R., Weimer, S., Mohr, C., DeCarlo, P. F., Gianini, M. F. D., Hueglin, C., Schneider, J., Favez, O., D'Anna, B., George, C., and Baltensperger, U.: Characterization of aerosol chemical composition with aerosol mass spectrometry in Central Europe: an overview, Atmos. Chem. Phys., 10, 10453-10471, https://doi.org/10.5194/acp-10-10453-2010, 2010.

Li, R., Wang, X., Gu, R., Lu, C., Zhu, F., Xue, L., Xie, H., Du, L., Chen, J., and Wang, W.: Identification and semi-quantification of biogenic organic nitrates in ambient particulate matters by UHPLC/ESI-MS, Atmos. Environ., 176, 140-147, https://doi.org/10.1016/j.atmosenv.2017.12.038, 2018.

Li, Y., Fu, T. M., Yu, J. Z., Yu, X., Chen, Q., Miao, R., Zhou, Y., Zhang, A., Ye, J., Yang, X., Tao, S., Liu, H., and Yao, W.: Dissecting the contributions of organic nitrogen aerosols to global atmospheric nitrogen deposition and implications for ecosystems, Natl. Sci. Rev., 10, 244, https://doi.org/10.1093/nsr/nwad244, 2023.

Lin, C., Huang, R.-J., Duan, J., Zhong, H., and Xu, W.: Primary and Secondary Organic Nitrate in Northwest China: A Case Study, Environ. Sci. Technol. Lett., 8, 947-953, https://doi.org/10.1021/acs.estlett.1c00692, 2021.

Mayorga, R., Xia, Y., Zhao, Z., Long, B., and Zhang, H.: Peroxy Radical Autoxidation and Sequential Oxidation in Organic Nitrate Formation during Limonene Nighttime Oxidation, Environ. Sci. Technol., 15337-15346, https://doi.org/10.1021/acs.est.2c04030, 2022.

Mensah, A. A., Holzinger, R., Otjes, R., Trimborn, A., Mentel, T. F., ten Brink, H., Henzing, B., and Kiendler-Scharr, A.: Aerosol chemical composition at Cabauw, The Netherlands as observed in two intensive periods in May 2008 and March 2009, Atmos. Chem. Phys., 12, 4723-4742, https://doi.org/10.5194/acp-12-4723-2012, 2012.

Minguillón, M. C., Perron, N., Querol, X., Szidat, S., Fahrni, S. M., Alastuey, A., Jimenez, J. L., Mohr, C., Ortega, A. M., Day, D. A., Lanz, V. A., Wacker, L., Reche, C., Cusack, M., Amato, F., Kiss, G., Hoffer, A., Decesari, S., Moretti, F., Hillamo, R., Teinilä, K., Seco, R., Peñuelas, J., Metzger, A., Schallhart, S., Müller, M., Hansel, A., Burkhart, J. F., Baltensperger, U., and Prévôt, A. S. H.: Fossil versus contemporary sources of fine elemental and organic carbonaceous particulate matter during the DAURE campaign in Northeast Spain, Atmos. Chem. Phys., 11, 12067-12084, https://doi.org/10.5194/acp-11-12067-2011, 2011.

Mohr, C., DeCarlo, P. F., Heringa, M. F., Chirico, R., Slowik, J. G., Richter, R., Reche, C., Alastuey, A., Querol, X., Seco, R., Peñuelas, J., Jiménez, J. L., Crippa, M., Zimmermann, R., Baltensperger, U., and Prévôt, A. S. H.: Identification and quantification of organic aerosol from cooking and other sources in Barcelona using aerosol mass spectrometer data, Atmos. Chem. Phys., 12, 1649-1665, https://doi.org/10.5194/acp-12-1649-2012, 2012.

Pikridas, M., Bougiatioti, A., Hildebrandt, L., Engelhart, G. J., Kostenidou, E., Mohr, C., Prévôt, A. S. H., Kouvarakis, G., Zarmpas, P., Burkhart, J. F., Lee, B. H., Psichoudaki, M., Mihalopoulos, N., Pilinis, C., Stohl, A., Baltensperger, U., Kulmala, M., and Pandis, S. N.: The Finokalia Aerosol Measurement Experiment – 2008 (FAME-08): an overview, Atmos. Chem. Phys., 10, 6793-6806, https://doi.org/10.5194/acp-10-6793-2010, 2010.

Poulain, L., Spindler, G., Birmili, W., Plass-Dülmer, C., Wiedensohler, A., and Herrmann, H.: Seasonal and diurnal variations of particulate nitrate and organic matter at the IfT research station Melpitz, Atmos. Chem. Phys., 11, 12579-12599, https://doi.org/10.5194/acp-11-12579-2011, 2011.

Rollins, A. W., Browne, E. C., Min, K. E., Pusede, S. E., Wooldridge, P. J., Gentner, D. R., Goldstein, A. H., Liu, S., Day, D. A., Russell, L. M., and Cohen, R. C.: Evidence for NO_x Control over Nighttime SOA Formation, Science, 337, 1210-1212, https://doi.org/doi:10.1126/science.1221520, 2012.

Rollins, A. W., Pusede, S., Wooldridge, P., Min, K. E., Gentner, D. R., Goldstein, A. H., Liu, S., Day, D. A., Russell, L. M., Rubitschun, C. L., Surratt, J. D., and Cohen, R. C.: Gas/particle partitioning of total alkyl nitrates observed with TD - LIF in Bakersfield, J. Geophys. Res.: Atmos., 118, 6651-6662, https://doi.org/10.1002/jgrd.50522, 2013.

Saarikoski, S., Carbone, S., Decesari, S., Giulianelli, L., Angelini, F., Canagaratna, M., Ng, N. L., Trimborn, A., Facchini, M. C., Fuzzi, S., Hillamo, R., and Worsnop, D.: Chemical characterization of springtime submicrometer aerosol in Po Valley, Italy, Atmos. Chem. Phys., 12, 8401-8421, https://doi.org/10.5194/acp-12-8401-2012, 2012.

Wang, Y., Hu, M., Guo, S., Wang, Y., Zheng, J., Yang, Y., Zhu, W., Tang, R., Li, X., Liu, Y., Le Breton, M., Du, Z., Shang, D., Wu, Y., Wu, Z., Song, Y., Lou, S., Hallquist, M., and Yu, J.: The secondary formation of organosulfates under interactions between biogenic emissions and anthropogenic pollutants in summer in Beijing, Atmos. Chem. Phys., 18, 10693-10713, https://doi.org/10.5194/acp-18-10693-2018, 2018.

Xu, L., Suresh, S., Guo, H., Weber, R. J., and Ng, N. L.: Aerosol characterization over the southeastern United States using high-resolution aerosol mass spectrometry: spatial and seasonal variation of aerosol composition and sources with a focus on organic nitrates, Atmos. Chem. Phys., 15, 7307-7336, https://doi.org/10.5194/acp-15-7307-2015, 2015.

Xu, W., Takeuchi, M., Chen, C., Qiu, Y., Xie, C., Xu, W., Ma, N., Worsnop, D. R., Ng, N. L., and Sun, Y.: Estimation of particulate organic nitrates from thermodenuder–aerosol mass spectrometer measurements in the North China Plain, Atmos. Meas. Tech., 14, 3693-3705, https://doi.org/10.5194/amt-14-3693-2021, 2021.

Yu, K., Zhu, Q., Du, K., and Huang, X.-F.: Characterization of Nighttime Formation of Particulate Organic Nitrates Based on High-Resolution Aerosol Mass Spectrometry in an Urban Atmosphere in China, Atmos. Chem. Phys., 19, 5235-5249, https://doi.org/10.5194/acp-19-5235-2019, 2019.

Zhu, Q., Cao, L.-M., Tang, M.-X., Huang, X.-F., Saikawa, E., and He, L.-Y.: Characterization of Organic Aerosol at a Rural Site in the North China Plain Region: Sources, Volatility and Organonitrates, Adv. Atmos. Sci., 38, 1115-1127, https://doi.org/10.1007/s00376-020-0127-2, 2021.